NATIONAL ADVISORY COMMITTEE FOR AERONAUTICS

TECHNICAL NOTE 2891

FACTORS AFFECTING LAMINAR BOUNDARY LAYER MEASUREMENTS IN A SUPERSONIC STREAM

By Robert E. Blue and George M. Low

Lewis Flight Propulsion Laboratory
Cleveland, Ohio

Washington
February 1953

NATIONAL ADVISORY COMMITTEE FOR AERONAUTICS

TECHNICAL NOTE 2891

FACTORS AFFECTING LAMINAR BOUNDARY LAYER MEASUREMENTS IN A SUPERSONIC STREAM

By Robert E. Blue and George M. Low

SUMMARY

The observed discrepancy at supersonic speeds between theoretical and apparent experimental average flat plate friction-drag coefficients calculated from boundary layer total-pressure surveys was investigated. Effects of the total-pressure probe, heat transfer through the leading-edge region, change in leading-edge radius and strength of the leading-edge wave, possible early transition to turbulent flow or "bursts of turbulence," and the slight streamwise pressure gradient inherent in flat plate flow were investigated for plates with very sharp leading edges.

Only one of these factors, the effect of the total-pressure probe, was found to be significant. Total-pressure probes of different tip heights, when placed in laminar boundary layers developing under identical conditions, were found to yield different values of friction-drag coefficient. Extrapolation of these measurements indicates that a probe of vanishing size would yield the theoretically predicted values of average flat plate friction-drag coefficients. A correlation describing the relation between the friction-drag discrepancy and the probe tip height is presented.

INTRODUCTION

Most available experimental values of average friction-drag coefficient for laminar flat plate flow have been obtained by total-pressure surveys of the boundary layer. Results reported in references 1 to 3 consistently indicate drag coefficients that are in the range of 10 to 100 percent higher than the values predicted by compressible laminar boundary layer theory. Other measurements made along the wall of a supersonic tunnel behind a boundary layer removal scoop (ref. 4) gave values that were even higher than those found in the investigations of references 1 to 3 at comparable conditions of Reynolds number.

The wide range of variability of the experimental results tends to rule out the possibility of attributing the discrepancy between theory and experiment to a deficiency in the theory alone. Furthermore, local friction coefficients determined from force measurements on a small element set in a plate surface show excellent agreement with boundary layer theory (ref. 5). The theory considers boundary layer growth on an infinitely thin flat plate starting at zero thickness at the leading edge and developing into a flow with zero pressure gradient. Experimentally, this situation can only be approximated. The precision to which any part or all of the physical situation hypothesized in the theory is reproduced may influence the size of the measured discrepancy.

An analysis of local friction coefficient based on the measured boundary layer Mach number distribution led the authors of reference 3 to conclude that the boundary layer air suffers a momentum loss near the plate leading edge. A consideration of the pressure distribution over the leading-edge region, based on the blunt-body theory of reference 6, shows that such a loss should occur and that it will be directly proportional to the radius of the edge. The discrepancies in average friction coefficient reported in reference 3 are at most $3\frac{1}{2}$ times larger than those shown in reference 1. The leading-edge radii, however, differed by a factor of 10. Consequently, factors other than the leading-edge pressure drag must be involved in the observed discrepancy.

The measured momentum discrepancy could be attributed to any of a number of causes, for example, heat transfer through the thin leading-edge region of the plate, momentary transition to turbulence, that is, "bursts of turbulence" (ref. 7), or an instrument error in the form of a probe interference effect or a misinterpretation of the pressure reading. It is the purpose of this report to present the findings of an investigation of these and other effects which might account for the difference between theory and experiment.

This investigation consisted principally of an experimental study of the boundary layer on a flat plate and an evaluation of the measuring technique. Total-pressure surveys of the boundary layer were made at Mach numbers of 2 and 3 over a range of Reynolds number at several distances from the plate leading edge. Several leading-edge radii were used on the flat plates and a systematic variation of total-pressure probe tip height was made. These measurements were made in two different test facilities at the NACA Lewis laboratory.
The authors are indebted to Mr. John W. Schwartzenberg for making many of the experimental measurements.

APPARATUS AND PROCEDURE

The boundary layer measurements were made on flat-plate models in two supersonic wind tunnels. Tunnel 1 had a test section of 3.84 by 10 inches and a nominal free-stream Mach number of 2. The test section of tunnel 2 measured 4 by 4 inches, and its nominal free-stream Mach number was 3. Air to both tunnels was supplied at a maximum stagnation pressure of 50 inches of mercury absolute. The supply air temperature (ahead of heaters) was -20° F for tunnel 1 and -70° F for tunnel 2, thus insuring a dew point sufficiently low to obtain condensation-free flow. The tunnels exhausted to a pressure of about 3 inches of mercury absolute.

All total pressures in the boundary layer were measured on a mercury well-type manometer. Static pressures were measured on butyl phthalate manometers with high vacuum reference pressures. Temperature measurements were indicated on a self-balancing potentiometer.

The test plate used in tunnel 1 was 6 inches long, 3.84 inches wide, and 0.25 inch thick. The plate used in tunnel 2 measured 8 by 4 by 0.25 inch. The top (test) surfaces of both plates were flat and the surface roughness did not exceed a value of 8 microinches rms. Rubber seals were provided between the plates and the tunnel side walls to prevent flow between the top and bottom surfaces.

The plate used in tunnel 1 had a leading-edge radius of curvature of less than 0.0005 inch, as determined on a comparator from a section of a molding plaster cast of the leading-edge region (a 50X magnification of the leading-edge region showed that the nose of the plate was nearly semicircular, so that definition of leading-edge radius was justified). The bottom surface of the plate was chamfered to an angle of 12° in the leading- and trailing-edge regions.

In order to determine the pressure gradient and the temperature along the plate, 15 static-pressure taps and 6 thermocouples were located in the plate surface, as shown in figure 1. The plate was supported by pivots and a sting in order to permit changes in angle of attack.

The radius of curvature of the leading edge of the plate used in tunnel 2 was less than 0.0005 inch for several tests, but a larger radius of curvature, of the order of 0.001 to 0.002 inch, was used in most of the tests. The bottom surface was chamfered to an angle of 10.6°. Static-pressure taps were installed in the plate surface 2.38 and 3.38 inches from the plate leading edge and 0.25 inch from the plate center line.

Details of the total-pressure probes used to survey the boundary layer are shown in figure 2. A range of probe tip heights from 0.003 to 0.016 inch is represented. Distance from the plate surface to the bottom of the probe tip was measured with a micrometer and is considered accurate to 0.0005 inch. Contact of the probe with the plate surface was indicated electrically (see ref. 1).

Only probe 3 (see table, fig. 2) was used in tunnel 1. Total-pressure surveys of the boundary layer were made with the probe tip located $\frac{1}{2}$, $1\frac{1}{2}$, and $2\frac{1}{2}$ inches from the plate leading edge with the plate at zero angle of attack, and with the probe tip located $2\frac{1}{2}$ inches from the leading edge at an angle of attack of -5°. For each probe location, the inlet stagnation pressure was varied from about 15 to 40 inches of mercury absolute. The inlet air was heated to a stagnation temperature ranging between 80° and 90° F.

Probes 1, 2, 4, and 5 were used in tunnel 2, and boundary layer surveys were made with the probe tip located $2\frac{3}{8}$ and $3\frac{3}{8}$ inches from the plate leading edge. The inlet stagnation pressure was varied from 20 to 40 inches of mercury absolute, while the inlet temperature was held at 102° F.

Plate static pressures and surface temperatures were recorded before and after each boundary layer survey. All surveys were started at the plate surface.

DATA REDUCTION

Calculation of momentum loss in the boundary layer requires the evaluation of mass flow ρu and momentum ρu^2 of the boundary layer air. In order to reduce the calculation steps required to obtain these quantities from the experimentally determined values of static and pitot pressure, the following dimensionless parameters were used (ref. 8):

$$\alpha = \frac{u}{\sqrt{RT}} \qquad \text{velocity parameter}$$

$$\beta = \frac{\rho u \sqrt{RT}}{p} \qquad \text{mass-flow parameter}$$

where T is the total temperature. (All symbols used in this report are defined in appendix A.) The mass-flow parameter was introduced in reciprocal form as a static-pressure parameter in reference 8. These

parameters can be shown to be uniquely determined by the ratio of static to pitot pressure p/H. The calculations of α, β, and $\alpha\beta = \rho u^2/p$ from p/H were made by IBM machines in the manner described in appendix B. Typical laminar boundary layer profiles of the velocity, mass-flow, and momentum parameters are shown in figures 3 to 5 for several Reynolds numbers. These data represent all the boundary layer surveys made with probe 4. Duplicate surveys under identical conditions are distinguished by open and solid points. There was a slight lack of reproducibility, as is apparent in these figures, for all the boundary layer surveys made.

The momentum thickness θ expressed in terms of the parameters α and β is

$$\theta = \int_0^{\delta} \frac{p}{p_1}\left(\frac{\beta}{\beta_1}\sqrt{\frac{T_1}{T}} - \frac{\alpha\beta}{\alpha_1\beta_1}\right) dy \qquad (1)$$

With the conventional assumption that static pressure is constant through the boundary layer, the ratio p/p_1 is 1. The distribution of total temperature is also required to evaluate the equation for θ. Because no temperature surveys were made, the simplifying assumption of a constant total temperature was used in all calculations. The effect of this assumption on the calculation of θ is discussed in the section Calculation Errors.

The total-pressure readings, assumed to exist at the geometric center of the tube, were taken at equally spaced distances from the plate surface. It was therefore possible to integrate the equation for θ numerically with the α and β calculated from the original data. Values for the integrals of β and $\alpha\beta$ were obtained for every other point of the original data using Stirling's rule.

A "running value" of momentum thickness θ_y was defined by replacing the free-stream quantities subscripted 1 in equation (1) with values measured at the ordinate y, denoted by a subscript y in equation (2), and carrying the integration out to the limit y.

$$\theta_y = \int_0^{y} \left(\frac{\beta}{\beta_y} - \frac{\alpha\beta}{\alpha_y\beta_y}\right) dy = \frac{1}{\beta_y}\int_0^{y} \beta\, dy - \frac{1}{\alpha_y\beta_y}\int_0^{y} \alpha\beta\, dy \qquad (2)$$

The ratios of pressure and temperature were eliminated in equation (2). by the assumptions of constant static pressure and total temperature through the boundary layer.

The method just described of calculating a profile of θ_y rather than predetermining the free-stream velocity and temperature or Mach

number as was done in references 1 to 3 shows the dependence of θ on the choice of free-stream conditions. The profiles of θ_y shown in figure 6 attain a peak value before reaching the edge of the boundary layer and then decrease, approaching a constant in the stream far from the plate surface. Values of θ used to calculate friction-drag coefficients were chosen at the point where the velocity gradient first became zero. Average flat plate friction coefficients were calculated from the Kármán momentum equation

$$2\frac{d\theta}{dx} + 2\theta\left(\frac{\frac{\delta^*}{\theta} + 2}{u_1}\frac{du_1}{dx} + \frac{1}{\rho_1}\frac{d\rho_1}{dx}\right) = \frac{\tau_w}{\rho_1\frac{u_1^2}{2}} = c_f \qquad (3)$$

Integration of c_f over a length of boundary layer run x yields the average friction-drag coefficient. For the case of a zero pressure gradient the momentum equation (3) may be readily integrated, yielding $C_f = 2\theta/x$ for the average friction-drag coefficient.

Experimental Errors

Static pressure. - Pressures measured with a differential manometer board using butyl phthalate as a working fluid can be read to an equivalent accuracy of better than ± 0.005 inch of mercury. For the range of static pressures in the test sections of the wind tunnels used for these measurements, this accuracy corresponded to a determination of the static pressure within ± 0.8 percent or less.

A calculation was made of the effect of an error in static pressure at a Mach number of 3 on the quantity $\frac{2\theta}{x}\sqrt{Re_x}$ using the theory of reference 9. Assumed values of Reynolds number, T_1, p, and x which were comparable with those of the experimental investigation were used to calculate a theoretical Mach number distribution through the boundary layer. A profile of p/H was then found from the Rayleigh equation and the Mach number distribution. Multiplication of the p/H curve by a new value of static pressure divided by the original assumed value gave a new distribution of p/H against y which was used to calculate a new value of θ in the manner described for a measured profile. A Reynolds number corresponding to the erroneous static pressure was also calculated. The results of this error calculation are presented in figure 7.

A similar error calculation was made using experimentally determined distributions of p/H rather than the theoretical profile of reference 4.

Curves showing the error in $\frac{2\theta}{x}\sqrt{Re_x}$ caused by an error in static pressure using measured profiles for two different probe sizes are also plotted in figure 7. The shape of the boundary layer profile apparently has a large effect on the error. The smallest probe used (probe 1), which measured a profile closest to that of the theory, shows the same trend of an error in $\frac{2\theta}{x}\sqrt{Re_x}$ with static-pressure error as does the error calculation made from the theoretical profile. The largest probe (probe 5), however, shows a reverse trend. By either of these calculations a reading error of 1 percent in static pressure will cause an error in $\frac{2\theta}{x}\sqrt{Re_x}$ of 1 percent or less.

Total-pressure recording. - The maximum possible error in the pressure measured by the pitot tube would be ±0.02 inch of mercury. This error would be randomly scattered through the readings taken during a boundary-layer survey. No attempt was made to calculate the error in θ due to such a random scatter. It was noted, however, that an error in the barometer reading, from which the total-pressure reading was subtracted, could be as large as 1/10 inch of mercury and still affect θ by less than 1/2 percent. In the absence of a method for specifically evaluating the effect of a random reading error, this result was assumed to indicate that an error in reading either the barometer or the total pressure could be neglected.

Turbulence level. - As shown in figure 1 of reference 10, tunnel 1 has a set of turbulence screens in the surge tank where the velocity is of the order of 8 feet per second. These screens are followed by a smooth contraction of 19 to 1 to the tunnel throat. The inlet to tunnel 2 consists of a 1-foot-diameter pipe connecting a 2-foot-diameter surge tank to a bellmouth. A contraction of 27 to 1 to the tunnel throat follows. A dirt filter made from 16 thicknesses of cheesecloth was placed across the connecting pipe at a point where the air velocity was about 70 feet per second.

A conclusion cannot be made regarding the levels of turbulence in the two tunnels from the measurements taken. The extreme difference in design, however, can be assumed to have caused substantially different levels. The agreement of the results obtained in these tunnels thus implies that turbulence level has no noticeable effect on θ, at least where the level of turbulence is reasonably low.

Total-pressure probe. - The possibility exists that a small total-pressure probe of the type used for boundary layer surveys consistently reads a value of total pressure that is in error, even out in the free stream. In order to determine whether such an error exists, a conventional blunt nose total-pressure probe, 1/8 inch in diameter, was

positioned with its center line 1/2 inch above the plate surface. The readings of this probe in comparison with the readings of the various boundary layer probes when they were located at the same position in the flow are shown in figure 8 for the five inlet pressures used in the number 2 tunnel measurements. The solid lines in the figure represent the readings of the 1/8-inch-diameter probe.

The boundary layer probe readings tend to scatter about a mean value slightly lower than that read by the large probe. The largest difference in total pressure measured by the two types of probe was 2 percent. This corresponds to approximately an 0.8 percent error in Mach number, α, β, or θ.

Yaw of total-pressure probe. - Each time a total-pressure probe is installed in the wind tunnel, it is necessary to realine the probe with the stream direction. This alinement was made both visually and by adjusting for the maximum total-pressure reading. Since this type of boundary layer total-pressure probe is relatively insensitive to angles of yaw in the free stream, it was difficult to be certain the probe was pointed precisely into the stream. Because the possibility that an angle of yaw might cause a more serious error when the probe is immersed in the velocity gradient of the boundary layer was recognized, a total-pressure survey was made for which the probe was deliberately misalined 3°. A running plot of momentum thickness against y for survey at 3° yaw is compared with the profile taken with the probe alined with the stream in figure 9. The two curves agree within less than the experimental reproducibility found for most of the boundary-layer surveys (see solid and open points of fig. 6). The actual error in alining the total-pressure probe was less than the 3° used in this error measurement for the effect of yaw.

Calculation Errors

Total-temperature assumption. - As previously stated it is necessary to assume some form of a total-temperature distribution through the boundary layer in order to calculate θ. All the calculations for this report assumed a constant total temperature. In order to evaluate the effect of this assumption on θ the theoretical Mach number distributions in the boundary layer as calculated from reference 9 were used to obtain the values of α and β necessary to integrate equation (2). The difference between calculated θ for a constant total temperature and theoretical θ is plotted in figure 10 in terms of the percentage error in θ against Mach number. A similar calculation was made with the assumption of a linear variation of total temperature between the theoretically predicted wall temperature and the free-stream total temperature. Errors due to this form of an assumed temperature distribution are also shown in figure 10. It is apparent in this case that the

simplest temperature assumption gives the best results. At a Mach number of 2 the error is nearly zero and it is still under 1 percent at a Mach number of 3.

Calculations near surface. - The typical boundary layer profiles of figures 3 and 4, showing the quantities β and $\alpha\beta$ plotted against y, show that the first few points measured near the plate surface do not fall on a smooth curve approaching the origin. (This has been tentatively attributed to interference between the probe and the plate surface.) Under the assumption that the velocity must go to zero at the plate surface, fairings neglecting these few apparently erroneous points were made. From these it was determined that either the fourth or the sixth points would lie on a straight line through the origin that fairs into the β curve and on a parabola through the origin that fairs into the $\alpha\beta$ curve. As explained in appendix B, this straight line and parabolic variation of β and $\alpha\beta$ was used in the integration of these quantities out to the fourth or sixth points. Beyond these points, Stirling's rule was used to integrate between the measured data points. This method of fairing is compatible with the theoretically predicted change in velocity and density near the plate surface. Since the velocity near the surface changes linearly while the density is nearly constant for the condition of zero heat transfer, the product ρu will vary almost linearly. The ρu^2 term, being the product of two linearly varying quantities, behaves as a parabola. Several calculations of θ starting at both the fourth and sixth points of a profile were made to see what difference the choice of starting point would have on θ. It was found to affect the calculated value of θ by about 0.5 percent.

Probe zero location. - An error in setting the zero location of the probe will cause an error in the integrals of β and $\alpha\beta$ as a result of the method of computation used for the first few points. This can be seen from the following sketch of β against y. The points which are eliminated from the calculation of θ by the fairing method are numbered 1, 2, and 3.

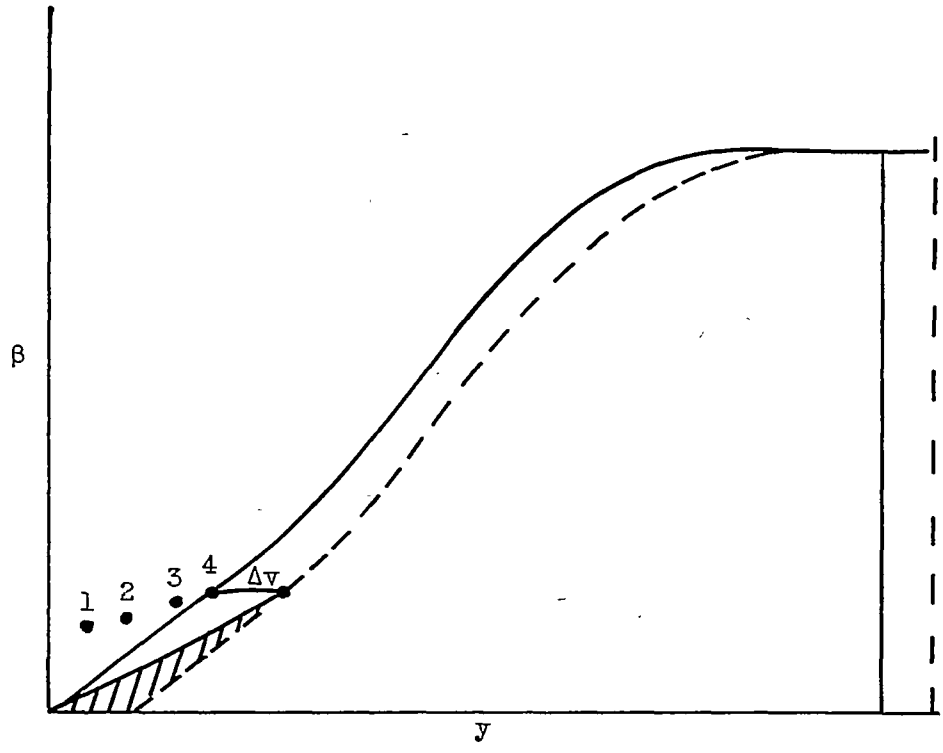

2756

If the zero setting is off by an amount Δy, the additional cross-hatched area bounded by the straight line to the origin and by the broken line, which is the original curve displaced by the error Δy, will be added to the integral of β. It is equal to $\beta_4 \frac{\Delta y}{2}$. Similarly, for $\alpha\beta$ the integral will be in error by $\alpha_4\beta_4 \frac{\Delta y}{3}$, so that the error in θ will be $\left(\frac{\beta_4}{2} - \frac{\alpha_4\beta_4}{3}\right) \Delta y$. The theoretical variation of β and $\alpha\beta$ computed from reference 9 for an average Reynolds number and Mach number of these experiments was used to calculate the percentage error in θ due to an error in y at zero for fairings starting at several distances from the wall. The results are plotted in figure 11. The error in locating the probe zero position for the present measurements was less than ± 0.0005 inch, which amounts to an error of ± 1 or 2 percent in θ for the range of starting points in y that was used.

The following table summarizes the maximum values of all possible errors in θ:

Cause of error	Error (percent)
Static pressure	±1.0
Total-pressure probe	-0.8
Total-temperature assumption	-0.7
Probe zero location	±1.6
Total error in θ	+1.1 -4.1

It was necessary to take the error in $\frac{2\theta}{x}\sqrt{Re_x}$ caused by an error in static pressure to be the same as the error in θ for this estimate. The reproducibility seen in figure 6 is within the range of this maximum total error.

RESULTS AND DISCUSSION

Average flat-plate friction-drag coefficients $2\theta/x$ were computed for all measured total-pressure profiles and are plotted against local stream Reynolds number Re_x on logarithmic coordinates in figure 12. A theoretical variation of $2\theta/x$ against Re_x obtained from reference 9 is also shown in figure 12 and applies for both $M_1 = 2$ and $M_1 = 3$ under the inlet temperature conditions of these tests. The measured values of $2\theta/x$ are from 5 to 65 percent higher than those predicted by theory. These high values of friction-drag coefficient might be attributed to transition to turbulent flow, to the slight longitudinal pressure gradient inherent to flow over a flat plate, to a momentum loss originating at the leading edge of the plate, to heat transfer through the leading-edge region, or to an effect of the total-pressure probe.

Transition from laminar to turbulent flow. - In order to determine the extent of the laminar boundary layer, the inlet stagnation pressure was varied while the total-pressure probe was held in a fixed position in the boundary layer. As long as the boundary layer is laminar, points on a plot of $\alpha\beta$ against the similarity parameter $y\sqrt{u_1/\nu_1 x}$ should fall near a universal curve regardless of the value of y. Any large deviation from this curve, which occurs at different values of $\alpha\beta$ depending on the distance y from the plate surface, indicates transition from laminar to turbulent flow. Typical transition curves obtained in tunnel 2 at $x = 3\frac{3}{8}$ inches are shown in figure 13 together with a conventional $\alpha\beta$ profile. Transition occurs at $Re_x \sim 10^6$. All results presented in this report were obtained at Reynolds numbers less than the transition Reynolds number as indicated by curves similar to figure 13.

The possibility that "bursts of turbulence" (ref. 7) are responsible for the momentum discrepancy while the mean value of the profiles did not exhibit transitional tendencies was also investigated. A low-range pressure transducer was connected to the total-pressure probe with the shortest possible length of tubing. The output of the transducer was fed through a preamplifier to an oscilloscope. The system could respond to pressure fluctuations as fast as 130 cycles per second. No pressure fluctuations, however, were detected at any point in that portion of the boundary layer where profiles were obtained. It therefore appears unlikely that momentary transition to turbulent flow existed in the Reynolds number range of these experiments.

Effect of pressure gradient. - Pressure distributions obtained on the flat plate in tunnel 1 are presented in figure 14. The initial expansion and following compression near the leading edge are characteristic of the flat plate flow and are not due to a tunnel disturbance. This fact was established by moving the plate upstream and downstream from the test position. The compression near the trailing edge, however, is caused by a tunnel disturbance, but it occurs 2 inches downstream of the last test station.

Although the actual pressure changes are minor, they occur over a short distance x, so that the pressure gradients are quite large. According to theory, a pressure gradient affects not only the momentum thickness but also the drag coefficient, which in the presence of a pressure gradient is not equal to $2\theta/x$, as can be seen from the Kármán momentum equation (eq. (3)).

Values of momentum thickness and drag coefficient for the pressure distributions presented in figure 14 were calculated by the method of reference 11 and compared with a zero pressure gradient solution. Results of this comparison showed that the effect of the pressure gradient on the momentum thickness was slight (1.6 percent), and that the error introduced by letting the drag coefficient equal $2\theta/x$ was also very small (2.4 percent).

Effect of leading edge. - If the discrepancy between theoretical friction-drag coefficients and measured drag coefficients is assumed to be due to an initial momentum defect which has been falsely attributed to friction, then a change in leading-edge geometry or a change in the strength of the leading-edge wave would be expected to change the magnitude of this discrepancy. The following tests were made to check this assumption:

The effect of the strength of the leading-edge wave was investigated in tunnel 1 by changing the angle of attack of the plate and thereby changing the strength of the shock wave. Because of tunnel choking

characteristics, the plate angle could be varied only between 0° and -5°. (A negative angle of attack yields a compression at the leading edge.)

A comparison of velocity profiles at angles of attack of 0° and -5° shows that the profiles were unaffected by this change in angle of attack (fig. 15). The abscissa in figure 15 is the similarity parameter $y\sqrt{u_1/\nu_1 x}$. Free-stream conditions for this comparison were selected behind the leading-edge shock wave. Drag coefficients, which are plotted in figure 12 also show no change with angle of attack.

It could be argued, however, that a detached wave stands ahead of the leading edge, and that the momentum defect caused by the pressure drag of the leading edge is responsible for the high measured drag coefficients. On this basis it is not surprising that the drag coefficients show no appreciable change with angle of attack, and it would be expected that the leading-edge geometry is of prime importance.

The plate in tunnel 2 was therefore tested with an exceedingly sharp leading edge ($r \lesssim 0.0005$) and with a somewhat duller leading edge ($0.001 < r < 0.002$). Velocity profiles obtained with both leading-edge configurations are presented in figure 16, and corresponding plots of θ_y against y are shown in figure 17. It is apparent that the difference between profiles obtained with the dull and sharp leading edges is of the same order of magnitude as the difference between repeat runs with the same leading edge (see figs. 3 and 6), and can therefore be attributed to lack of reproducibility of experimental data. It can be concluded that increasing the leading-edge radius from about 0.0005 to about 0.0015 inch has little or no effect on the measured drag coefficient.

It is thus reasonable to assume that the discrepancies between theoretical and measured drag coefficients found in this investigation are not caused by a momentum defect originating in the immediate vicinity of the leading edge.

Effect of heat transfer. - The measured flat-plate drag coefficients have been compared with theoretical drag coefficients for an insulated flat plate. This comparison is not strictly valid because there will be local heat transfer through the leading edge from the chamfered side of the plate to the top of the plate. An estimate based on the theory of reference 9 shows, however, that the effect of this heat transfer on skin friction is about 0.2 percent and hence may be neglected. The temperature along the surface of the plate in tunnel 1 varied by less than 3° F. Temperature recovery factors based on this surface temperature had a value of 0.88, which is in good agreement with previous experiments on insulated plates.

Effect of probe tip height. - The effect of the total-pressure probe on measured friction-drag coefficients was investigated by surveying the boundary layer under identical conditions with four probes which had outside probe tip heights h ranging from 0.003 to 0.016 inch. It was found most convenient to correlate results of these measurements on the basis of the difference between measured and theoretical friction-drag coefficients.

This difference $2(\theta - \theta_T)/x$ was first plotted against u_1/ν_1, which is a function of only the tunnel inlet conditions, and for given values of x and h, $2(\theta - \theta_T)/x$ was found to be independent of u_1/ν_1. Typical curves of $2(\theta - \theta_T)/x$ against u_1/ν_1 are shown in figure 18. There is, of course, a large amount of scatter, but it should be remembered that an error of about 2 percent in θ will cause an error of up to 30 percent in $2(\theta - \theta_T)/x$, depending on the magnitude of $2(\theta - \theta_T)/x$. It is evident, however, that there is no definite trend or variation of points in figure 18, and that, in the range of Reynolds number investigated, $2(\theta - \theta_T)/x$ can be considered constant as long as h and x remain constant. The arithmetic mean of all points taken with a given probe at a given station was therefore found, and henceforth only this mean value of $2(\theta - \theta_T)/x$ will be used.

A plot of the average friction-drag discrepancy $2(\theta - \theta_T)/x$ against probe tip height h is presented in figure 19. A straight line is faired through each set of points representing a constant distance x from the leading edge. The expression

$$\frac{2(\theta - \theta_T)}{x} = K(x)\, h^{0.64} \tag{4}$$

represents all points reasonably well. Because h is the only variable between points at a given station, equation (4) establishes that the greater part, or perhaps all, of the discrepancy between measured and theoretical friction-drag coefficients is caused by the finite height of the total-pressure probe tip. It is evident, however, that this probe effect depends also on the distance from the leading edge.

In order to determine quantitatively this dependency on x, measurements were made in tunnel 1 at three values of x with a constant probe tip height. A logarithmic plot of the average friction-drag discrepancy factor against distance from the leading edge is shown in figure 20. Points are well represented by a straight line of the form

$$\frac{2(\theta - \theta_T)}{x} = kx^{-1.22} \tag{5}$$

According to equation (4), this may be generalized to other probe heights by allowing k to be a function of h.

It is interesting to note that the exponent of $1/x$ in equation (5) is nearly twice the exponent of h in equation (4). This fact immediately suggests a correlation on the basis of h/x^2. It was found that the coefficients of h in equation (4) and of x in equation (5) are compatible, so that for corresponding values of h and x the values computed from both equations will agree.

Both sets of data were therefore combined and the friction-drag discrepancy factor $2(\theta - \theta_T)/x$ was plotted on logarithmic coordinates against h/x^2. The straight line

$$\frac{2(\theta - \theta_T)}{x} = 0.02\left(\frac{h}{x^2}\right)^{0.64} \tag{6}$$

was faired through all data points (fig. 21).

The points plotted in figure 21 represent a range in Reynolds number from 10^5 to 10^6, a range of x from 1/2 to $3\frac{3}{8}$ inches, and a range in probe tip height from 0.003 to 0.016 inch, and were obtained at Mach numbers of 2 and 3. Each point in this figure corresponds to the arithmetic mean of from 5 to 10 measured profiles, so that more than 60 individual boundary layer surveys are represented. Therefore no doubt remains that the friction-drag discrepancy factor as given by equation (6) is valid for flat plate friction-drag coefficients obtained under the aforementioned conditions.

It should be pointed out, however, that the final correlation was based on the parameter $(h/x^2)^{0.64}$, and that the coefficient of $(h/x^2)^{0.64}$ in equation (6) is therefore not dimensionless. A correlation based on hd/x^2, where d is the width of the probe opening, would be dimensionally correct and compatible with equation (6) because d was not varied appreciably in the present tests. If the probe effect is assumed to be primarily one of interference, then the skin-friction discrepancy factor would be expected to approach zero as d approached zero. But it is unlikely that a correlation based on the probe tip area hd could be valid for all tip shapes. Thus, the complete correlation factor might be a function of both hd/x^2 and a nondimensional shape factor.

A comparison with results of references 3 and 12 shows that such an additional factor is required in the correlation equation (6). The three points from reference 3, plotted in figure 21, were obtained at

three different values of x with one value of h. The point from reference 12 (also shown in fig. 21) represents the arithmetic mean of several points obtained at constant h and x, but at different values of u_1/ν_1. It is interesting to note that the friction-drag discrepancy factor for the results of reference 12 was again independent of u_1/ν_1 for $Re_x < 10^6$. The results of both references are considerably higher than the friction-drag discrepancy factor found in the present study. It appears quite possible that a probe tip shape factor could bring about agreement for all data, but no such factor can be predicted without a systematic variation of probe tip width.

On the other hand, the fact that the leading-edge radius of the plate used in reference 3 was considerably larger than that of the present tests may also account for the difference in results.

Of further interest is the fact that if the exponent in equation (6) were 2/3 instead of 0.64, an equation of the following form would result:

$$2(\theta - \theta_T) = K \left(\frac{h}{\sqrt{x}}\right)^{2/3} \tag{7}$$

where K is again dimensional. The factor $h/\sqrt{x}$ appears to be meaningful because all boundary layer variables increase proportionally to $\sqrt{x}$. These same variables are also a function of u_1/ν_1, however, so that the significance of equation (7) is not clear at present.

A theoretical explanation of the probe effect is beyond the scope of the present report. It is reasonable to believe that both a distortion of the boundary layer caused by the presence of the probe and the fact that the probe is in a shear flow rather than a uniform flow contribute to the discrepancy. Neither a displacement of the effective center of the probe of the magnitude predicted in reference 13 nor an area weighting of the pressure field ahead of the probe can account for the high measured values of θ. The effect of viscosity on probe reading (ref. 14) appears to be important only near the plate surface, where the measured points were replaced by a faired curve to the origin, so that the momentum thickness remains unaffected.

The fact that the momentum discrepancy factor is independent of u_1/ν_1 is in itself difficult to explain. At any given station the boundary layer thickness changes as u_1/ν_1 is varied. At the same time, however, the total-pressure gradient in the boundary layer also changes. It is not known how these and other factors combine to yield a constant value of $2(\theta - \theta_T)/x$.

An examination of $\alpha\beta$ and θ_y profiles for various probe tip heights at constant Reynolds number also fails to yield a satisfactory explanation of the probe effect. Typical profiles are shown in figures 22 and 23. The $\alpha\beta$ profiles for probes 1 and 4 are very similar in shape, while the profile for probe 5 exhibits a shift to the right. The peak near the edge of the boundary layer which is present in two of the profiles becomes more apparent as the probe tip height is increased. This peak is also present in the θ_y profiles (fig. 23), but in general it occurs within the boundary layer. All correlations presented herein are based on values of θ_y obtained at the value of y where $\partial u/\partial y$ first vanishes.

An examination of the factors to which might be attributed the discrepancy between measured and theoretical friction-drag coefficients has therefore shown that only one of these factors, namely, the probe effect, leads to a positive result. The fact that profiles measured under identical conditions but with probes of different tip heights yield distinctly different values of θ is evidence enough to establish this effect. A correlation as given by equation (6) further indicates that the entire friction-drag discrepancy may be attributed to the probe effect, and that if a hypothetical probe of vanishing tip height were employed, theoretical values of θ would be measured.

Further substantiation of the conclusion that the friction-drag discrepancy may be attributed to the probe effect is obtained from reference 5, where the results of direct measurements of local skin-friction coefficients using the floating-element technique are reported. These measurements were made at a Mach number of 2.55 on a flat plate with a leading-edge radius of less than 0.0005 inch. Local skin-friction coefficients, when plotted against a Reynolds number based on the distance x from the leading edge, agree exactly with the theory of Chapman and Rubesin for $M_1 = 2.55$. Average friction-drag coefficients obtained by integrating these local values would therefore also agree with theory. Thus, a friction-drag discrepancy factor of zero is obtained when no probe is present in the boundary layer.

CONCLUDING REMARKS

Pressure-probe measurements were made in the laminar boundary layer developing on a flat plate at free-stream Mach numbers of 2 and 3. High average measured flat-plate friction-drag coefficients, which had previously been observed, were again found in the present study.

Possibilities for error such as the effect of the total-pressure probe on boundary layer measurements, heat transfer through the leading-edge region, a change in leading-edge radius and the strength of the

leading-edge wave, and the possibility of early transition to turbulent flow or "bursts of turbulence" were investigated for plates with very sharp leading edges. Of these factors, only the probe effect led to positive results.

Total-pressure probes of different tip heights placed in a laminar boundary layer developing under identical conditions were found to measure different values of average friction-drag coefficients. An empirical correlation of these measurements indicates that a probe of vanishing height would measure the theoretically predicted values of average flat plate friction-drag coefficients.

Lewis Flight Propulsion Laboratory
National Advisory Committee for Aeronautics
Cleveland, Ohio, November 14, 1952

APPENDIX A

SYMBOLS

The following symbols are used in this report:

C_f	average friction-drag coefficient, $\frac{1}{\frac{1}{2}\rho_1 u_1^2}\int_0^x \tau_w dx$
c_f	local friction-drag coefficient (eq. (3))
H	pitot pressure
h	outside height of probe tip
K,k	constants of proportionality
M	Mach number
P	total pressure
p	static pressure
p_0	unperturbed pressure used in error calculations
R	gas constant
Re_x	local stream Reynolds number based on distance x
r	radius of curvature of leading edge
T	total temperature
t	ambient temperature
u	velocity in x-direction
x	chordwise distance measured from leading edge parallel to stream
y	distance measured perpendicular to plate surface
α	dimensionless velocity parameter
β	dimensionless mass-flow parameter

δ^*	boundary layer displacement thickness
η_t	temperature recovery factor
θ	boundary layer momentum thickness
$\varkappa$	parameter defined by eq. (B8)
ν	kinematic viscosity
ρ	mass density
τ	shear stress

Subscripts:

1	free-stream conditions
M	measured quantity
s	upstream stagnation conditions
T	laminar boundary layer theory
w	conditions at plate surface
y	conditions evaluated at distance y from plate surface

APPENDIX B

REDUCTION OF DATA

By Jack M. Lande

The experimental data were evaluated by IBM machines utilizing a system of data reduction capable of handling many classes of gas flow problems. The application of this system to the reduction of boundary layer data is discussed herein. Although only the case of the laminar boundary layer with constant static pressure and constant total temperature was considered in the main part of the report, the method of calculation presented in this appendix applies to both laminar and turbulent boundary layers with varying static pressure and total temperature.

In general, the following quantities are measured in boundary layer studies:

$H(y)$ pitot pressure

$p(y)$ static pressure

$T_M(y)$ measured temperature

Velocity and temperature profiles, in addition to momentum and displacement thickness, are desired as a result of calculations. The calculations can be greatly simplified with the aid of the following nondimensional quantities (ref. 8):

$$\alpha = \frac{u}{\sqrt{RT}} \tag{B1}$$

$$\beta = \frac{\rho u \sqrt{RT}}{p} \tag{B2}$$

$$\alpha\beta = \frac{\rho u^2}{p} \tag{B3}$$

Each of these quantities is uniquely related to the ratio p/H.

The momentum and displacement thicknesses for $\partial p/\partial y = 0$ and $\partial T/\partial y \neq 0$ become

$$\theta = \frac{\sqrt{T_1}}{\beta_1} \int \frac{\beta}{\sqrt{T}}\, dy - \frac{1}{\alpha_1 \beta_1} \int \alpha\beta\, dy \tag{B4}$$

$$\delta^* = \int \left(1 - \frac{\beta}{\beta_1} \sqrt{\frac{T_1}{T}}\right) dy \tag{B5}$$

The momentum thickness θ is no longer significant in the calculation of skin friction for $\partial p/\partial y \neq 0$; in this case the integral $\int (\alpha\beta + 1)p \, dy$ is required.

The first step in the calculation of the aforementioned quantities is the temperature and manometer fluid correction of measured pressures and the determination of p/H.

Calculation of α. - The velocity parameter α is related to p/H by the isentropic flow equation

$$\alpha^2 = 7\left[1 - \left(\frac{p}{H}\right)^{-\frac{2}{7}}\right] \tag{B6}$$

for Mach numbers less than 1, and by the Rayleigh equation

$$\left(\frac{p}{H}\right)^2 = \frac{(36\alpha^2 - 7)^5 (7 - \alpha^2)^2}{(36)^6 \alpha^{14}} \tag{B7}$$

for Mach numbers greater than 1. (The ratio of specific heats γ was taken as 1.4 in eqs. (B6) and (B7).)

The difficulties inherent in calculating α from these expressions are overcome by the definition and calculation of an intermediate quantity $\varkappa$ which is defined by

$$\alpha = \sqrt{2(1 - p/H)}\left[1 + \varkappa(1 - p/H)\right] \tag{B8}$$

A table deck of $\varkappa$ and the slope of $\varkappa$ at a given point as a function of p/H can be prepared with the aid of equations (B6) to (B8).

For a given boundary layer profile, $\varkappa$ can then be obtained for each value of p/H by linear interpolation in the table deck. Finally, α is obtained by substitution of corresponding values of $\varkappa$ and p/H into equation (B8).

Calculation of β. - The quantities α and β can be related through the equation of state

$$p = \rho R t \tag{B9}$$

and the one-dimensional energy equation, which can be expressed as

$$\frac{t}{T} = 1 - \frac{\gamma - 1}{2\gamma} \alpha^2 \tag{B10}$$

For a constant value of specific heat and $\gamma = 1.4$, equations (B1), (B9), and (B10) yield the following expression for β:

$$\beta = \frac{7\alpha}{7 - \alpha^2} \tag{B11}$$

This expression was used to calculate β from previously determined values of α.

Calculation of $\alpha\beta$. - The product of equations (B1) and (B11) gives for $\alpha\beta$

$$\alpha\beta = \frac{7\alpha^2}{7 - \alpha^2} \tag{B12}$$

Calculation of $\beta/\sqrt{T}$. - The measured temperature T_M is related to the local static temperature by

$$\frac{T_M}{t} = 1 + \frac{\gamma - 1}{2} \eta_t M^2 \tag{B13}$$

where η_t is the temperature probe recovery factor. The following expression is obtained from equations (B13) and (B10) and the definitions of $\alpha\beta$:

$$\frac{\beta}{\sqrt{T}} = \sqrt{\frac{\left(1 + \frac{\gamma - 1}{2\gamma} \eta_t \alpha\beta\right)\alpha\beta}{T_M}} \tag{B14}$$

Calculation of integrals. - The integrations of the quantities $\beta/\sqrt{T}$, $\alpha\beta$, and $\alpha\beta p$ at a distance from the wall are carried out using Stirling's parabolic rule for both the laminar and turbulent cases. Near the wall, however, where data points are unreliable, two different procedures are required for the laminar and turbulent cases.

Because the velocity profile near the wall for a laminar boundary layer is nearly linear, and because the density under conditions of zero heat transfer is nearly constant, the following expressions are used:

$$\left.\begin{aligned} \beta &= ay \\ \alpha\beta &= by^2 \end{aligned}\right\} \quad \text{(B15)}$$

These results, together with the assumption of constant p and T, are therefore used to evaluate the integrals for the first points in a laminar boundary layer.

For turbulent boundary layers the form of β and $\alpha\beta$ near the wall is determined empirically. The following expressions, based on available turbulent boundary layer data, are suggested for β:

$$\left.\begin{aligned} \beta &= a_1 y^{1/2} + a_2 y + a_3 y^{3/2} + a_4 y^2 \\ \text{or} \\ \beta &= y^{1/N}\left(a_1 y + a_2 y^2 + a_3 y^3 + a_4 y^4\right) \end{aligned}\right\} \quad \text{(B16)}$$

The quantity $\alpha\beta$ is usually well represented by

$$\alpha\beta = b_1 y + b_2 y^2 + b_3 y^3 + b_4 y^4 \quad \text{(B17)}$$

Equations (B16) and (B17) together with the assumptions of constant static pressure and constant total temperature are used to evaluate the integrals for the points near the wall in the turbulent case.

Combinations of these integrals yield the momentum thickness θ and the displacement thickness δ^*.

Significant digits. - All calculations are carried out to five or more digits, which is sufficient in relation to the instrumentation used in obtaining the experimental data.

Calculation time. - The actual machine time required to obtain results for a given boundary layer profile is minor. It has been found, however, that data obtained during a given morning's wind tunnel run (about 4 profiles of about 35 points each) can be reduced by one operator during the afternoon of the same day. In that manner results of a set of tests are known before the next set of tests is begun. Many more profiles could be handled at the same time, but for the present tests the feature of immediate data analysis outweighed the economy of accumulating a great amount of data before reduction was begun.

REFERENCES

1. Blue, Robert E.: Interferometer Corrections and Measurements of Laminar Boundary Layers in Supersonic Stream. NACA TN 2110, 1950.

2. Higgins, Robert W., and Pappas, Constantine C.: An Experimental Investigation of the Effect of Surface Heating on Boundary-Layer Transition on a Flat Plate in Supersonic Flow. NACA TN 2351, 1951.

2756

3. Maydew, Randall C., and Pappas, Constantine C.: Experimental Investigation of the Local and Average Skin Friction in the Laminar Boundary Layer on a Flat Plate at a Mach Number of 2.4. NACA TN 2740, 1952.

4. Monaghan, R. J., and Johnson, J. E.: The Measurement of Heat Transfer and Skin Friction at Supersonic Speeds. Part II. Boundary Layer Measurements on a Flat Plate at M = 2.5 and Zero Heat Transfer. Tech. Note AERO. 2031, Sup. 99, British R.A.E., Dec. 1949. (Superseded by A.R.C. CP 64, 1952.)

5. Coles, Donald: Direct Measurement of Supersonic Skin Friction. Jour. Aero. Sci., vol. 19, no. 10, Oct. 1952, p. 717.

6. Moeckel, W. E.: Approximate Method for Predicting Form and Location of Detached Shock Waves Ahead of Plane or Axially Symmetrical Bodies. NACA TN 1921, 1949.

7. Emmons, H. W.: The Laminar-Turbulent Transition in a Boundary Layer - Part I. Jour. Aero. Sci., vol. 18, no. 7, July 1951, pp. 490-498.

8. Turner, L. Richard, Addie, Albert N., and Zimmerman, Richard H.: Charts for the Analysis of One-Dimensional Steady Compressible Flow. NACA TN 1419, 1948.

9. Chapman, Dean R., and Rubesin, Morris W.: Temperature and Velocity Profiles in the Compressible Laminar Boundary Layer with Arbitrary Distribution of Surface Temperature. Jour. Aero. Sci., vol. 16, no. 9, Sept. 1949, pp. 547-565.

10. Brinich, Paul F.: Boundary-Layer Measurements in 3.84- by 10-Inch Supersonic Channel. NACA TN 2203, 1950.

11. Low, George M.: Simplified Method for Calculation of Compressible Laminar Boundary Layer with Arbitrary Free-Stream Pressure Gradient. NACA TN 2531, 1951.

12. Bradfield, W. S., DeCoursin, D. G., and Blumer, C. B.: Characteristics of Laminar and Turbulent Boundary Layer at Supersonic Velocity. Res. Rep. No. 83, Dept. Aero. Eng., Inst. Tech., Univ. Minn., July 1952. (AMC Contract No. AF-33-(038)-12918.)

13. Young, A. D., and Maas, J. N.: The Behavior of a Pitot Tube in a Transverse Total-Pressure Gradient. R. & M. No. 1770, 1937.

14. Chambré, P. L., and Smith, H. R.: The Impact Tube in a Viscous Compressible Gas. Rep. No. HE-150-63, Dept. Eng., Univ. Calif. (Berkeley), Aug. 29, 1949. (Contract No. N7-ONR-295-Task 3.)

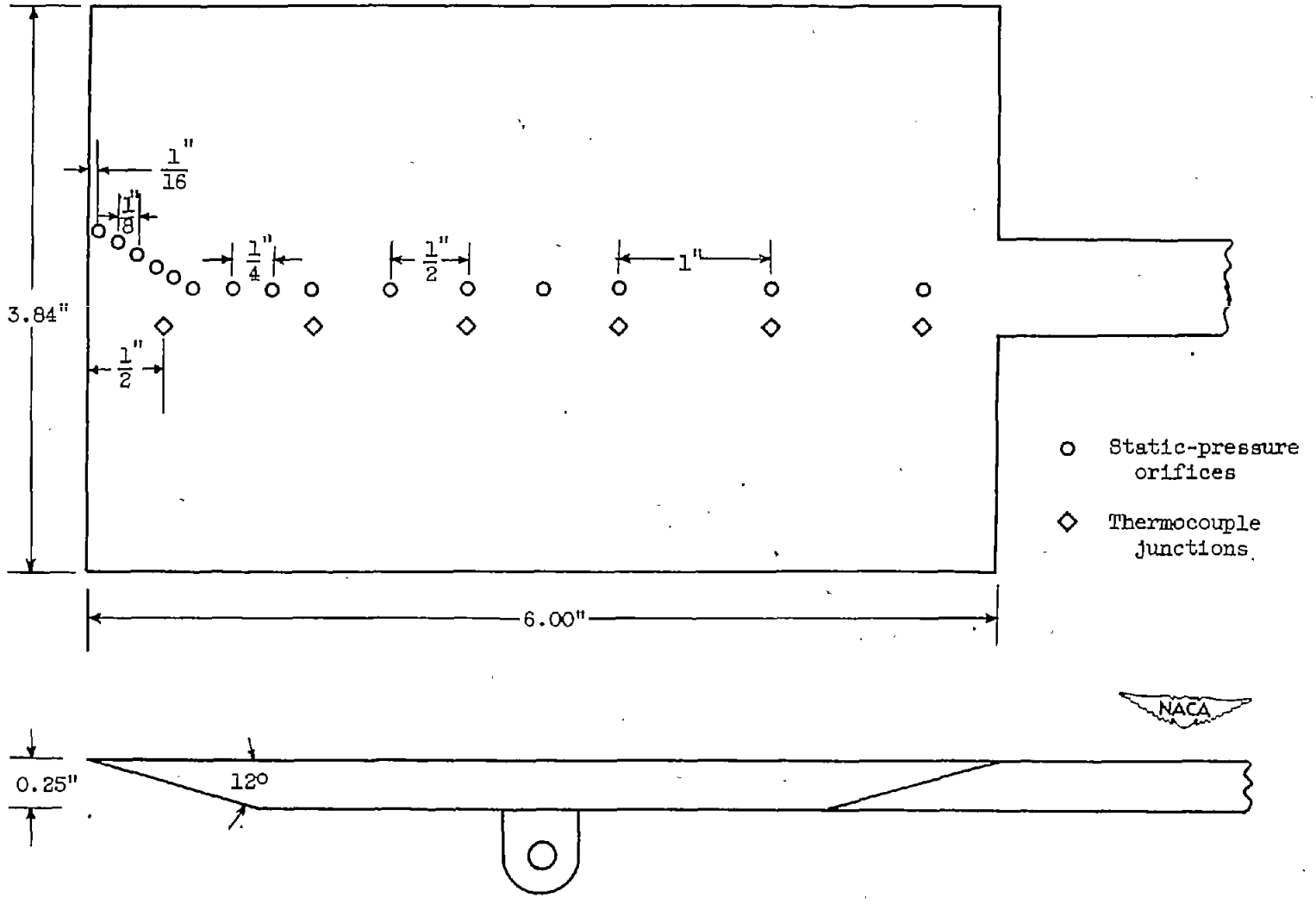

Figure 1. - Sketch of flat plate model used in tunnel 1.

Probe	Dimensions (in.)			
	a	b	h	d
1	0.001	0.001	0.003	0.05
2	.001	.002	.005	.05
3	.002	.002	.006	.04
4	.004	.002	.008	.04
5	.012	.002	.016	.04

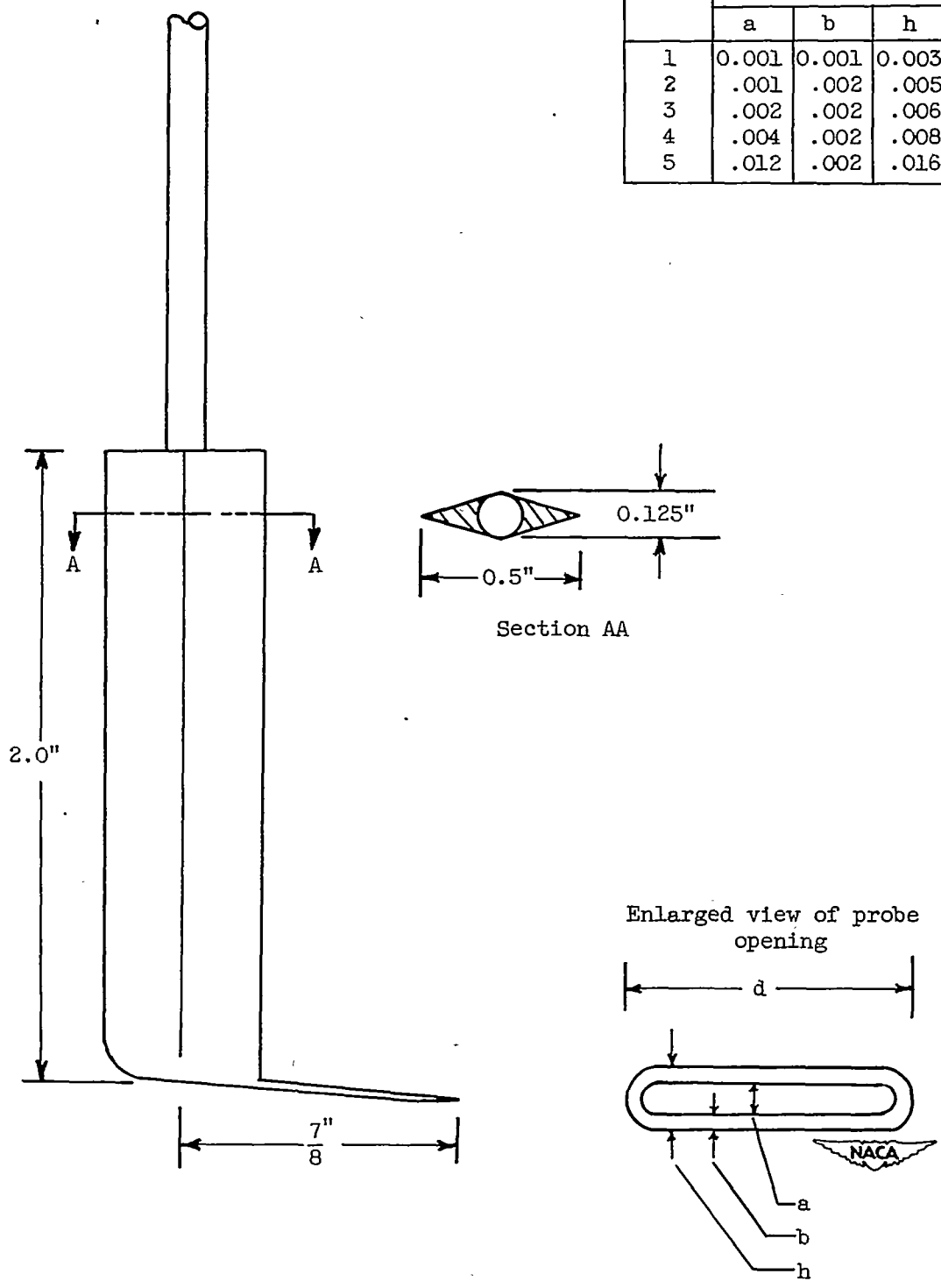

Figure 2. - Total-pressure probe.

2756

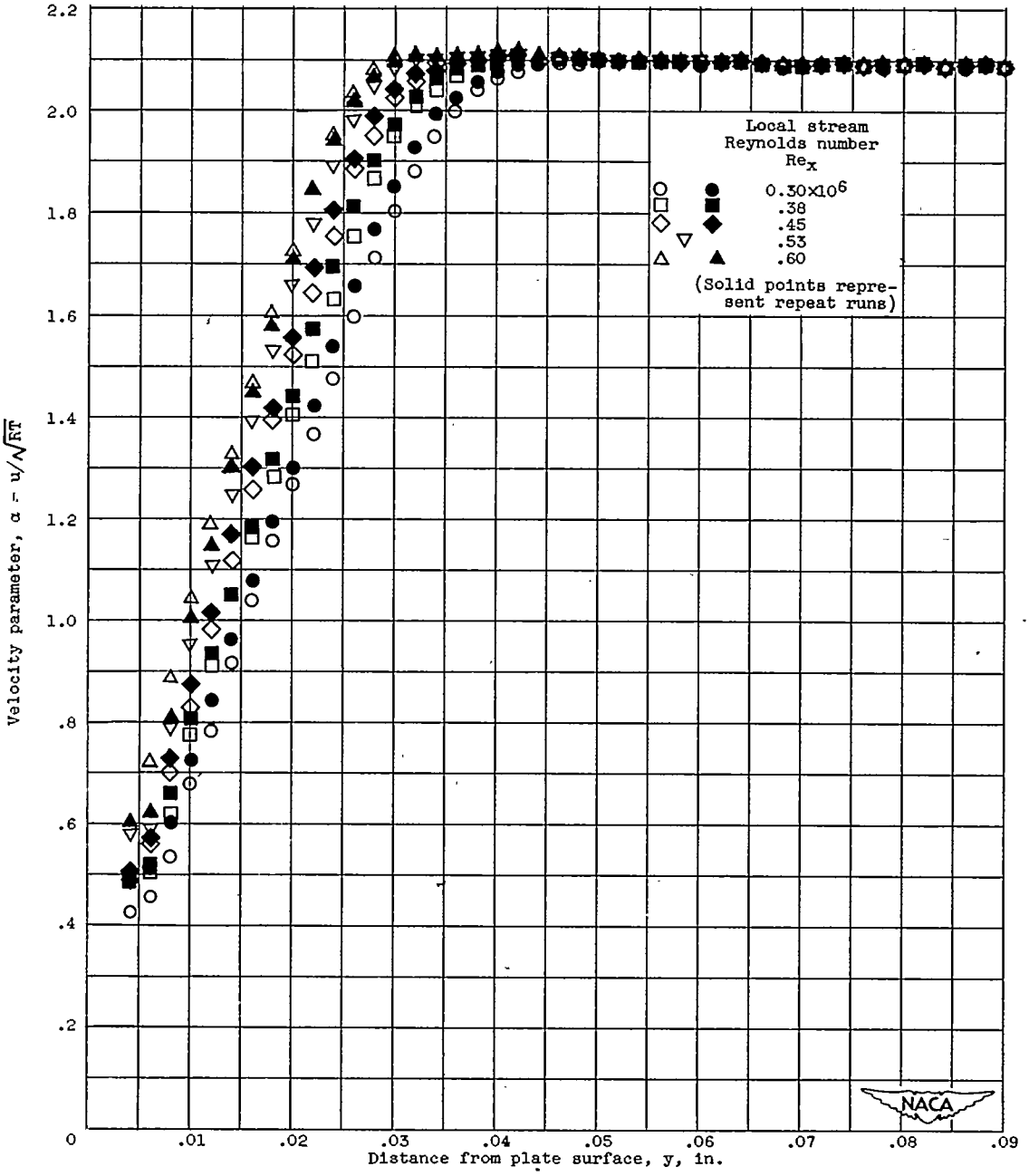

Figure 3. - Typical velocity parameter profiles. Distance from leading edge, 2.38 inches; probe tip height, 0.008 inch; free-stream Mach number, 3.

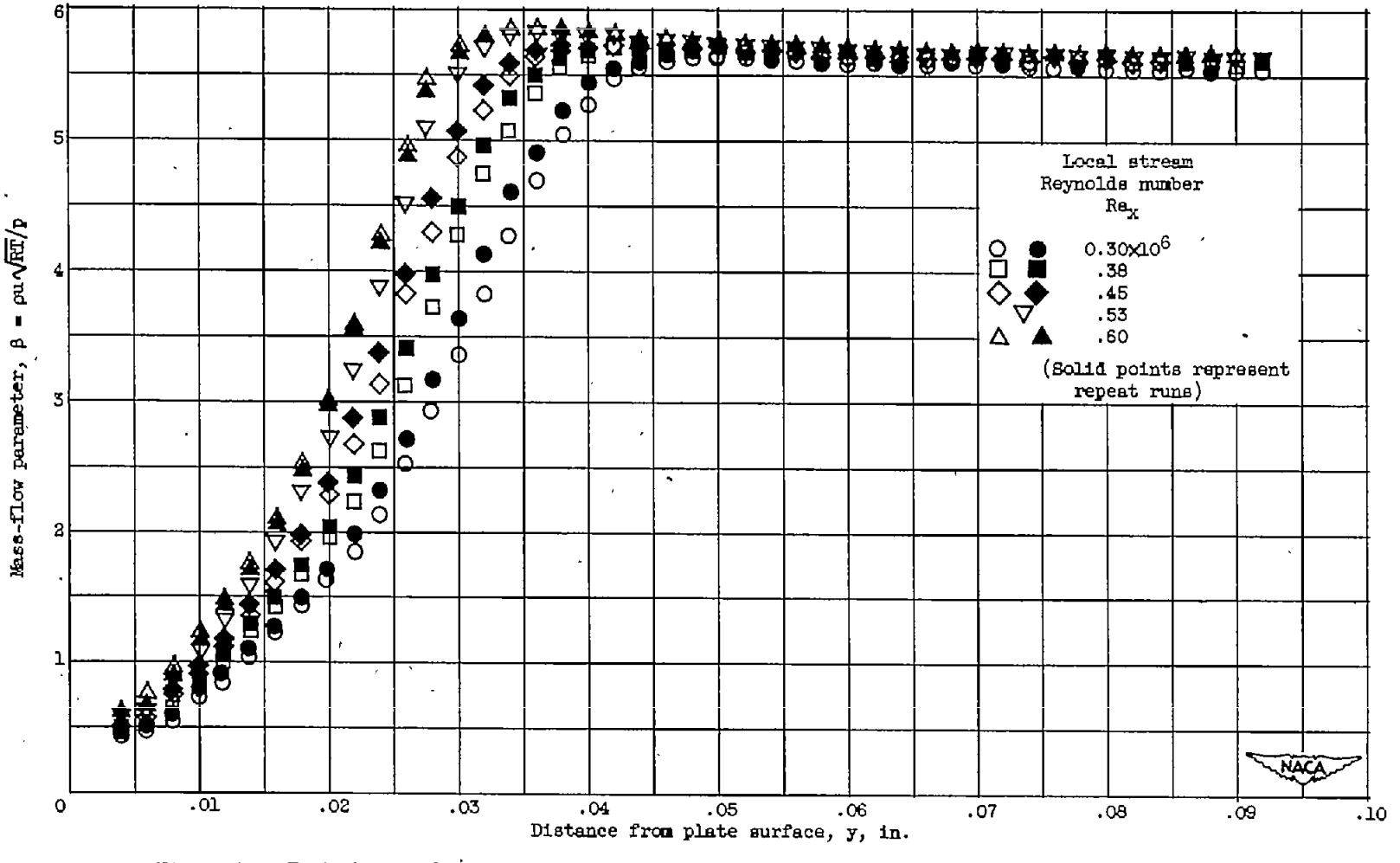

Figure 4. - Typical mass-flow parameter profiles. Distance from leading edge, 2.38 inches; probe tip height, 0.008 inch; free-stream Mach number, 3.

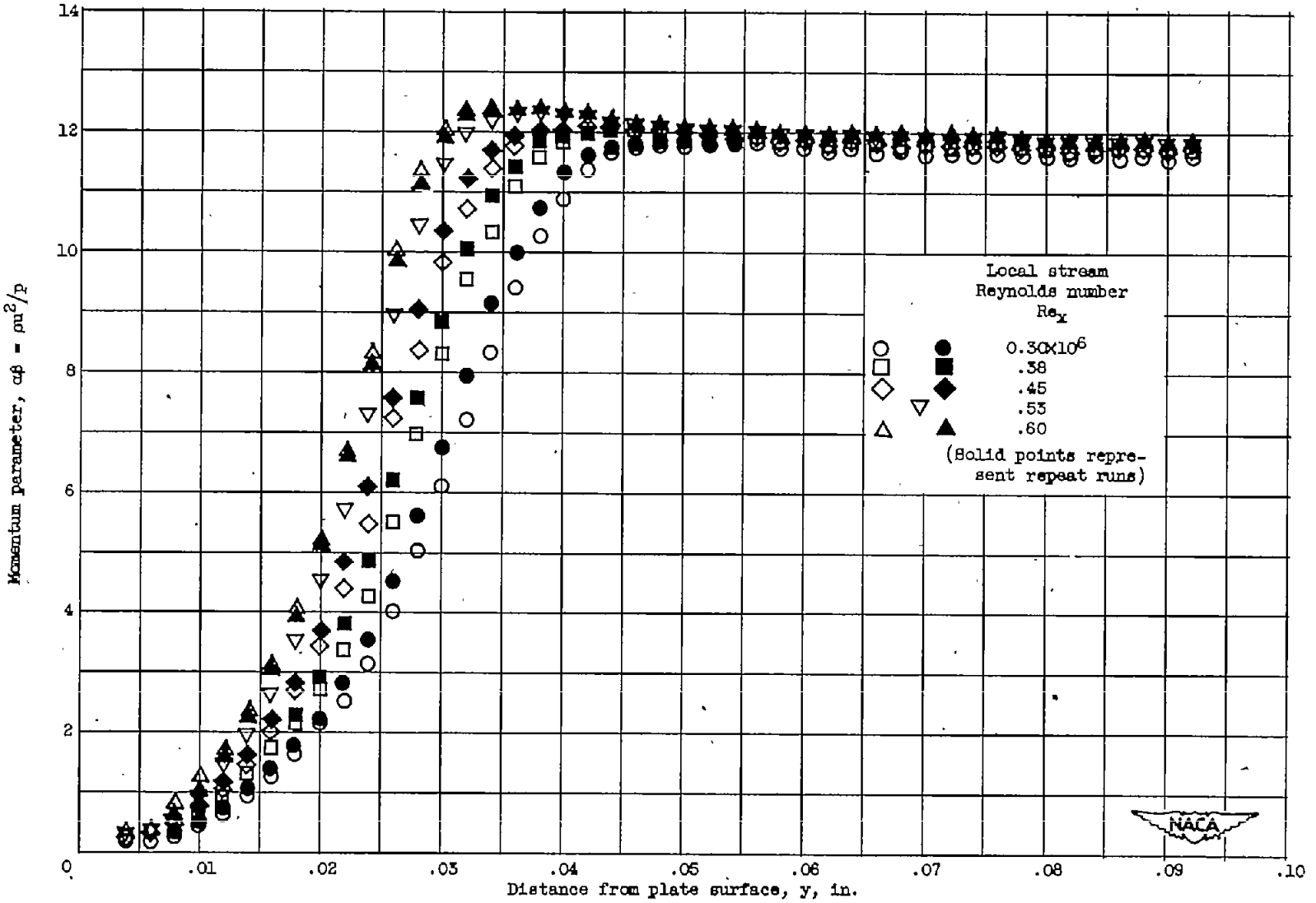

Figure 5. - Typical momentum parameter profiles. Distance from leading edge, 2.38 inches; probe tip height, 0.008 inch; free-stream Mach number, 3.

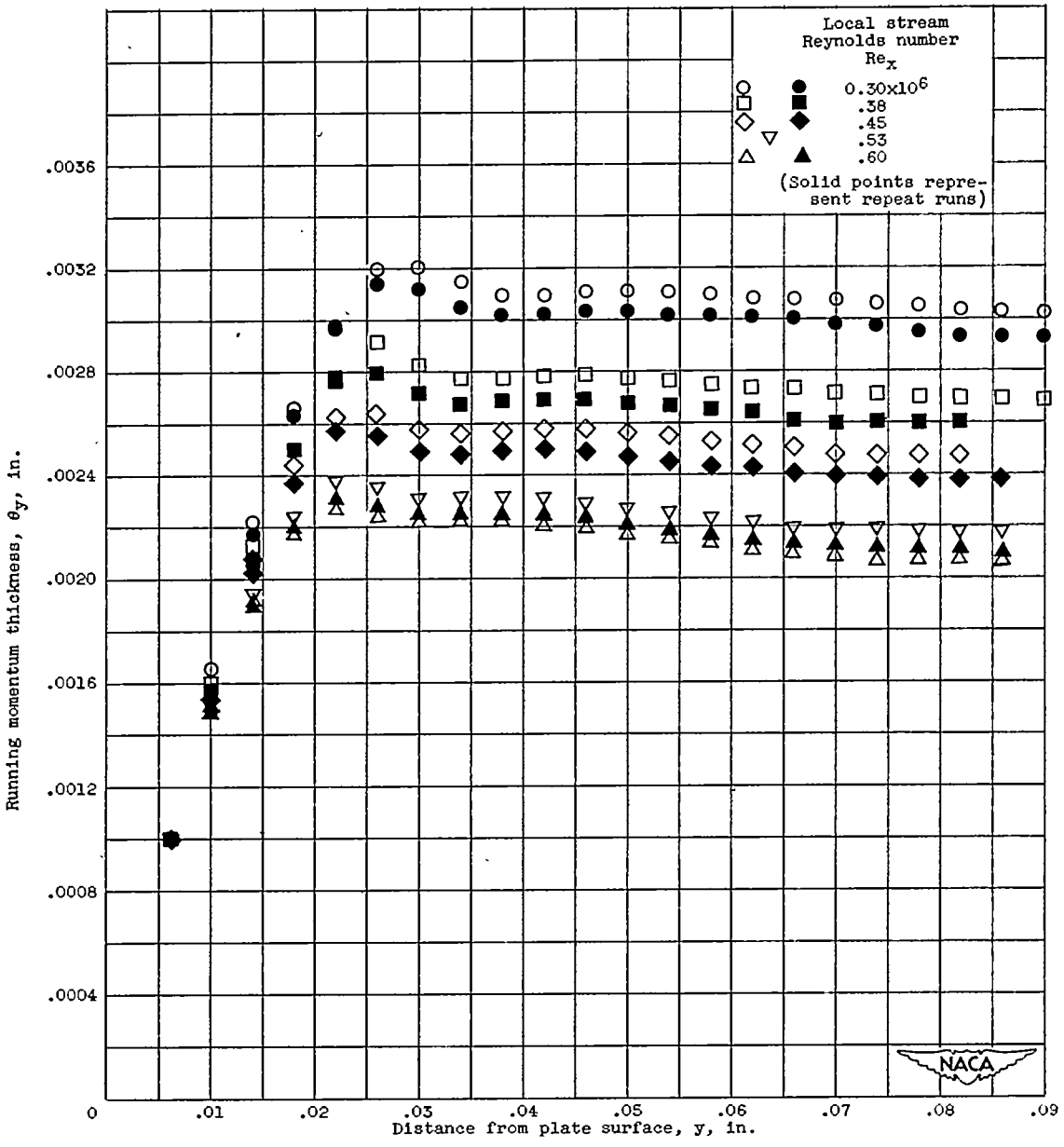

Figure 6. - Typical momentum thickness profiles. Distance from leading edge, 2.38 inches; probe tip height, 0.008 inch; free-stream Mach number, 3.

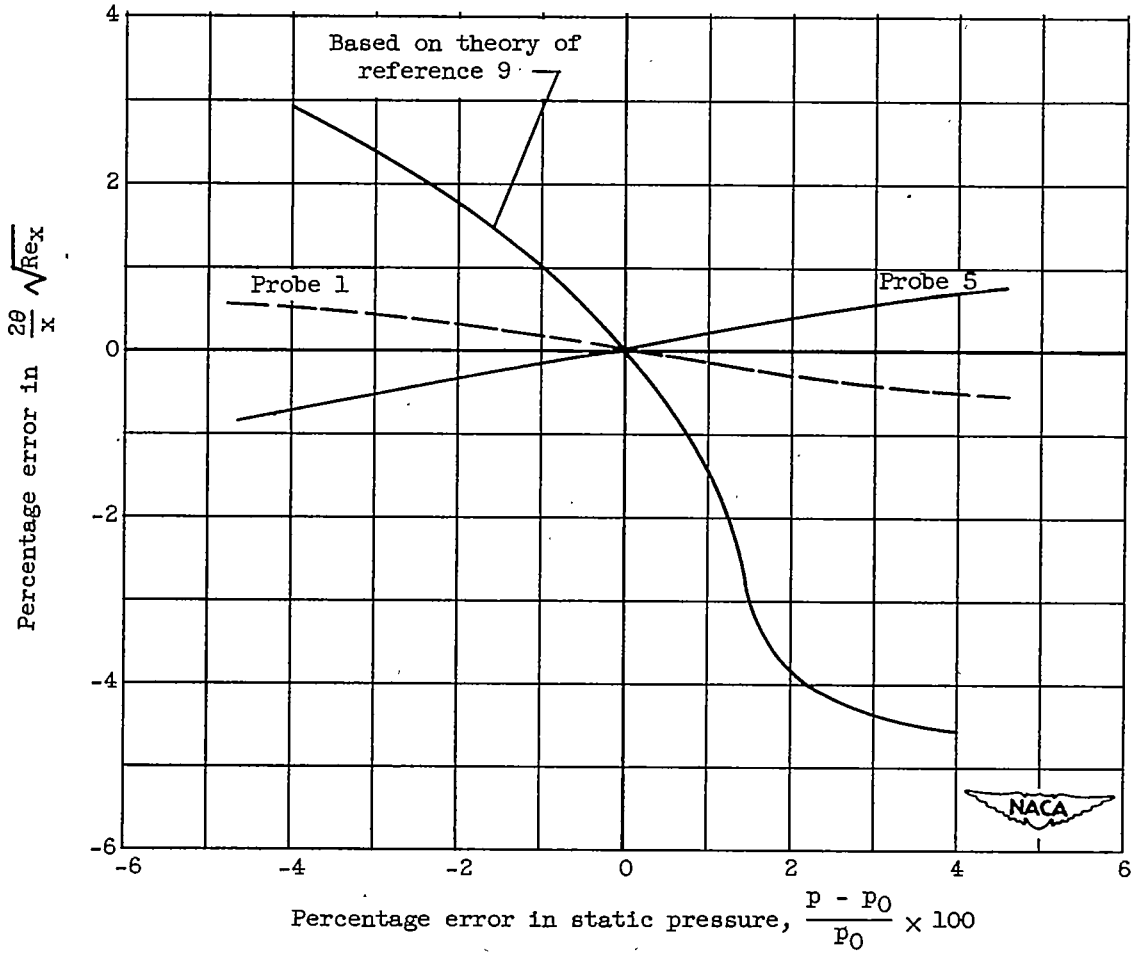

Figure 7. - Effect of error in static pressure on $\frac{2\theta}{x}\sqrt{Re_x}$. Free-stream Mach number, 3.

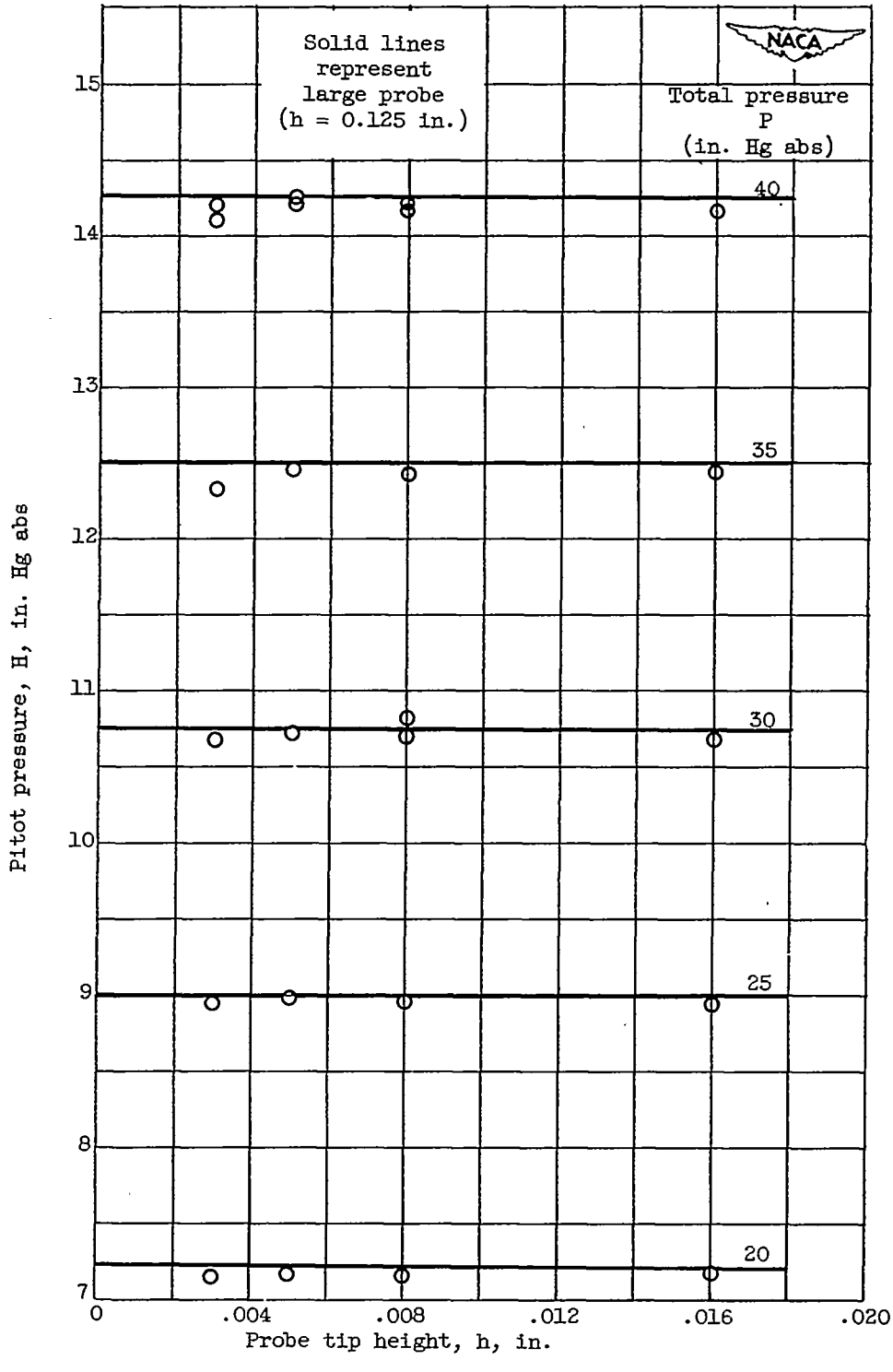

Figure 8. - Pitot pressure in free stream. Distance from leading edge, 2.38 inches; distance from plate surface, 0.5 inch; free-stream Mach number, 3.

2756

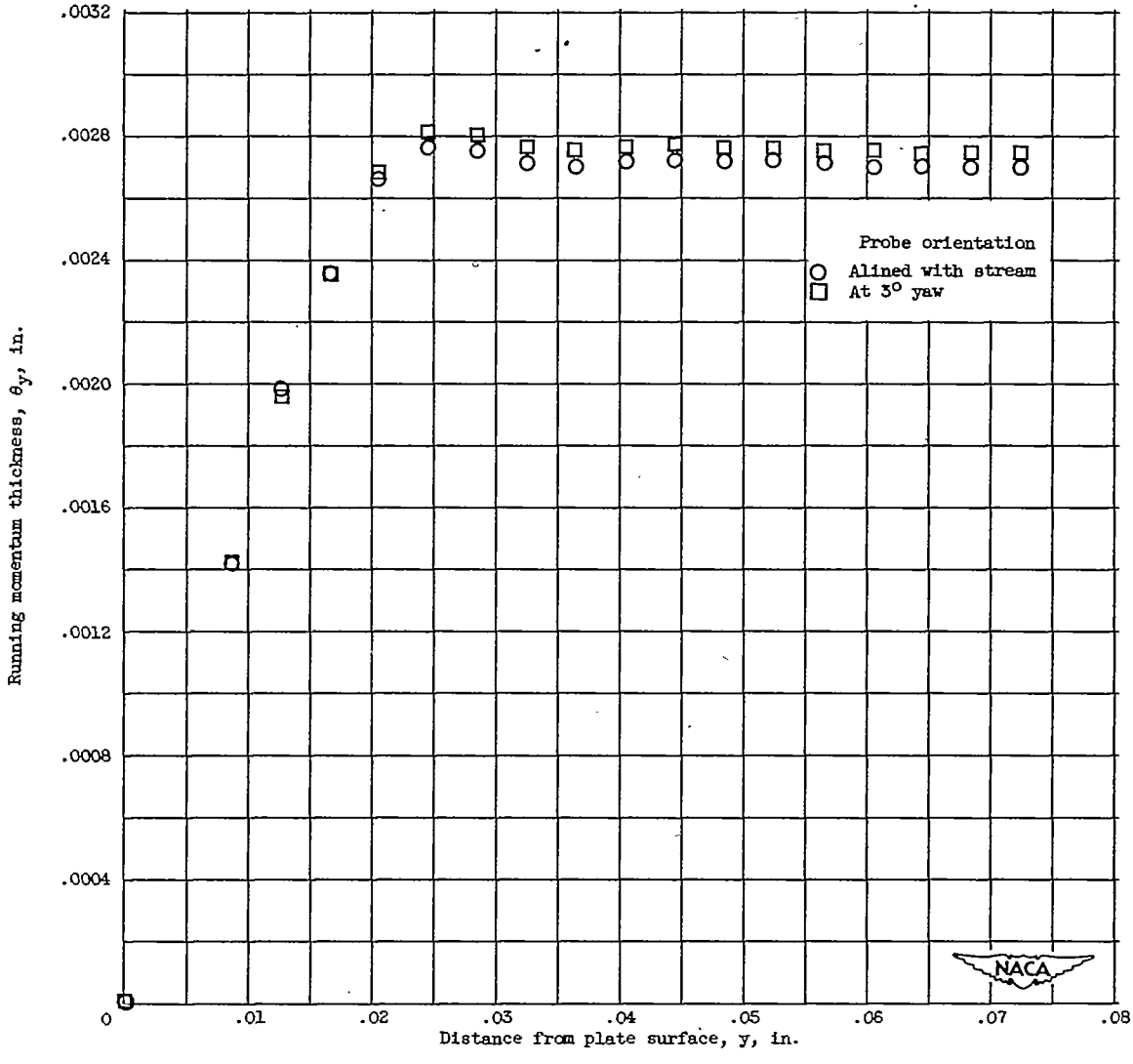

Figure 9. - Effect of total-pressure probe yaw on measured momentum thickness. Free-stream Mach number, 3.

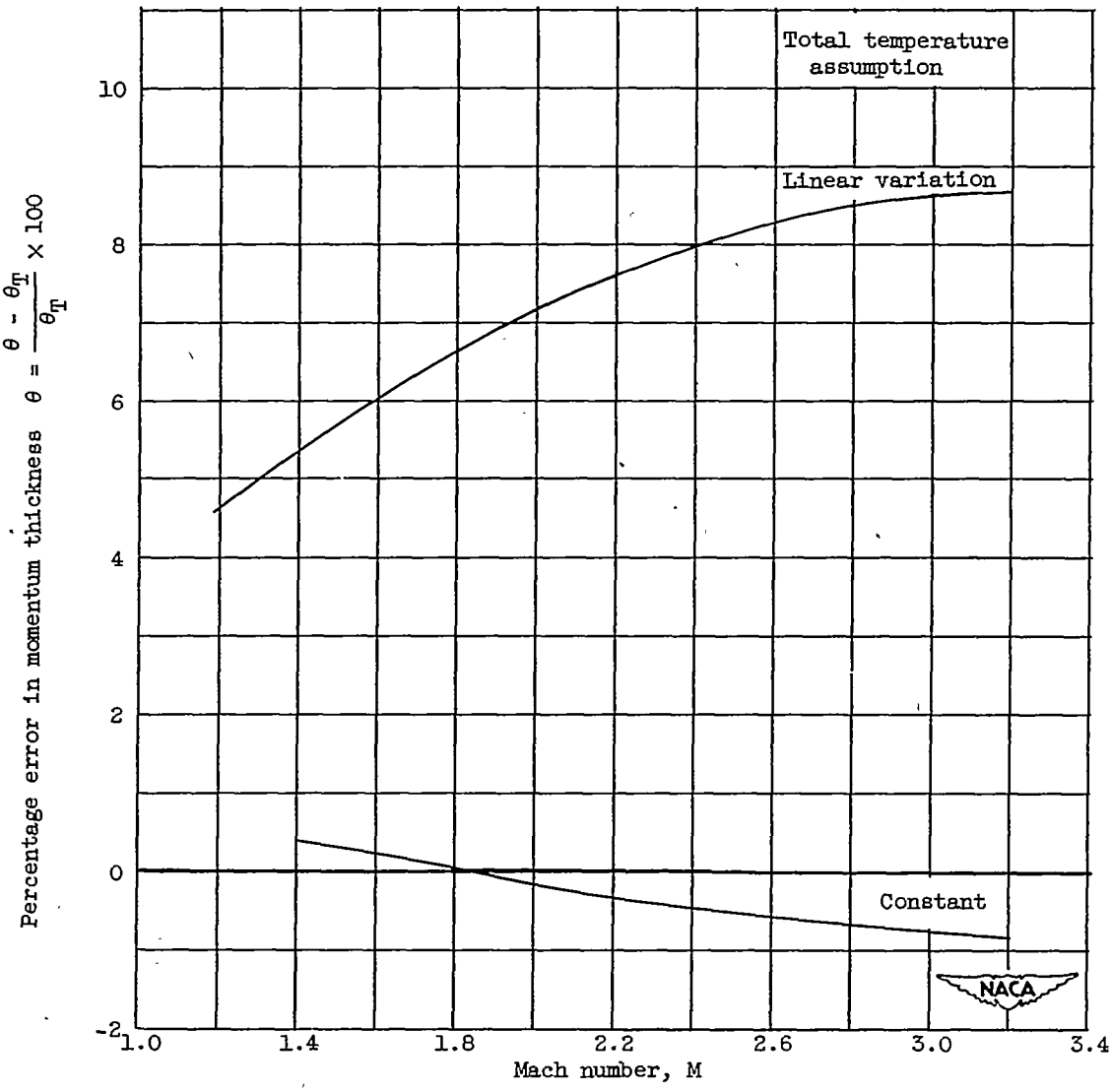

Figure 10. - Error in computing momentum thickness caused by total-temperature assumption.

2756

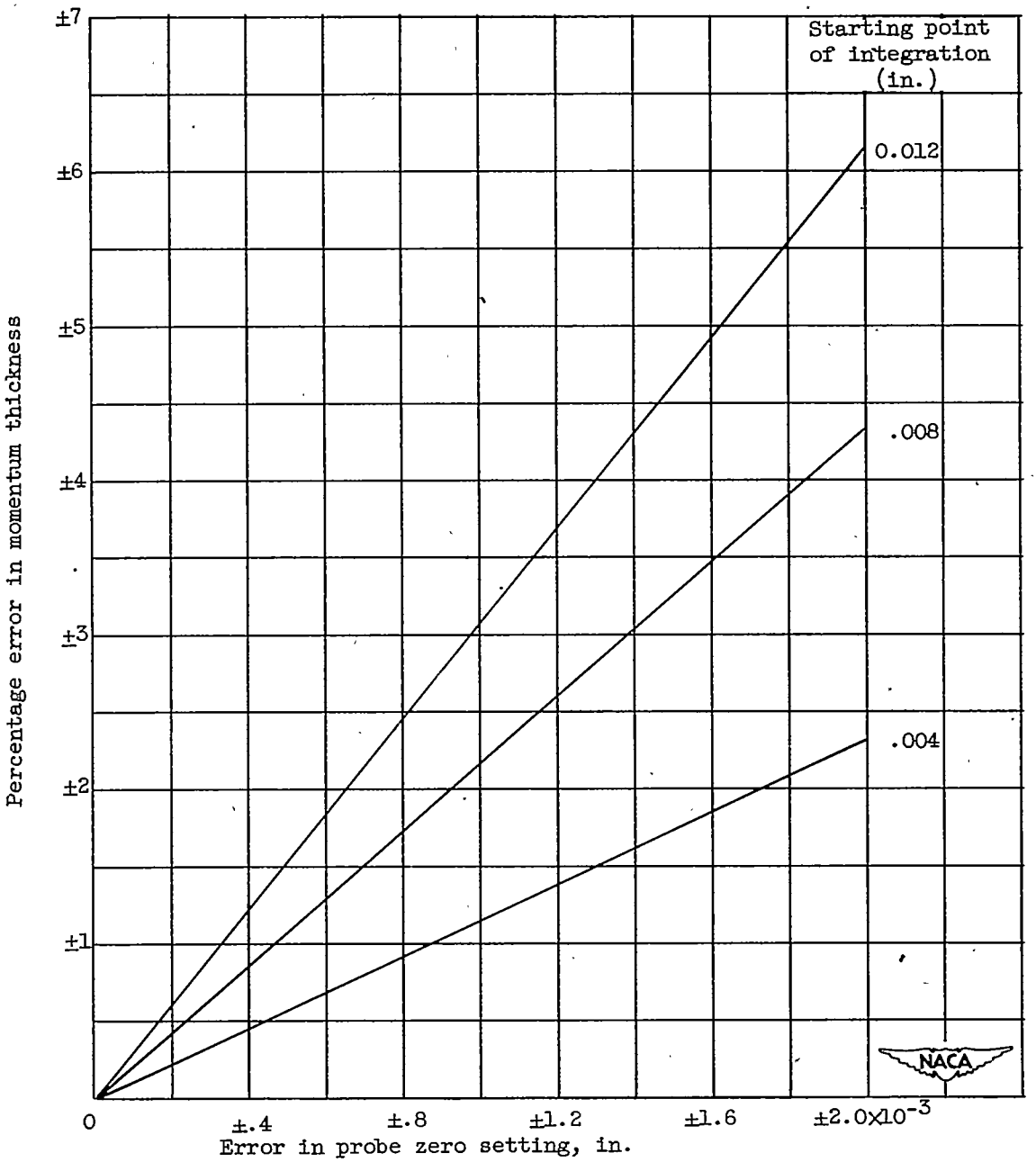

Figure 11. - Effect of error in probe zero setting on momentum thickness. Based on theory of reference 9. Distance from leading edge, 2.38 inches; free-stream Mach number, 3; local stream Reynolds number, 450,000.

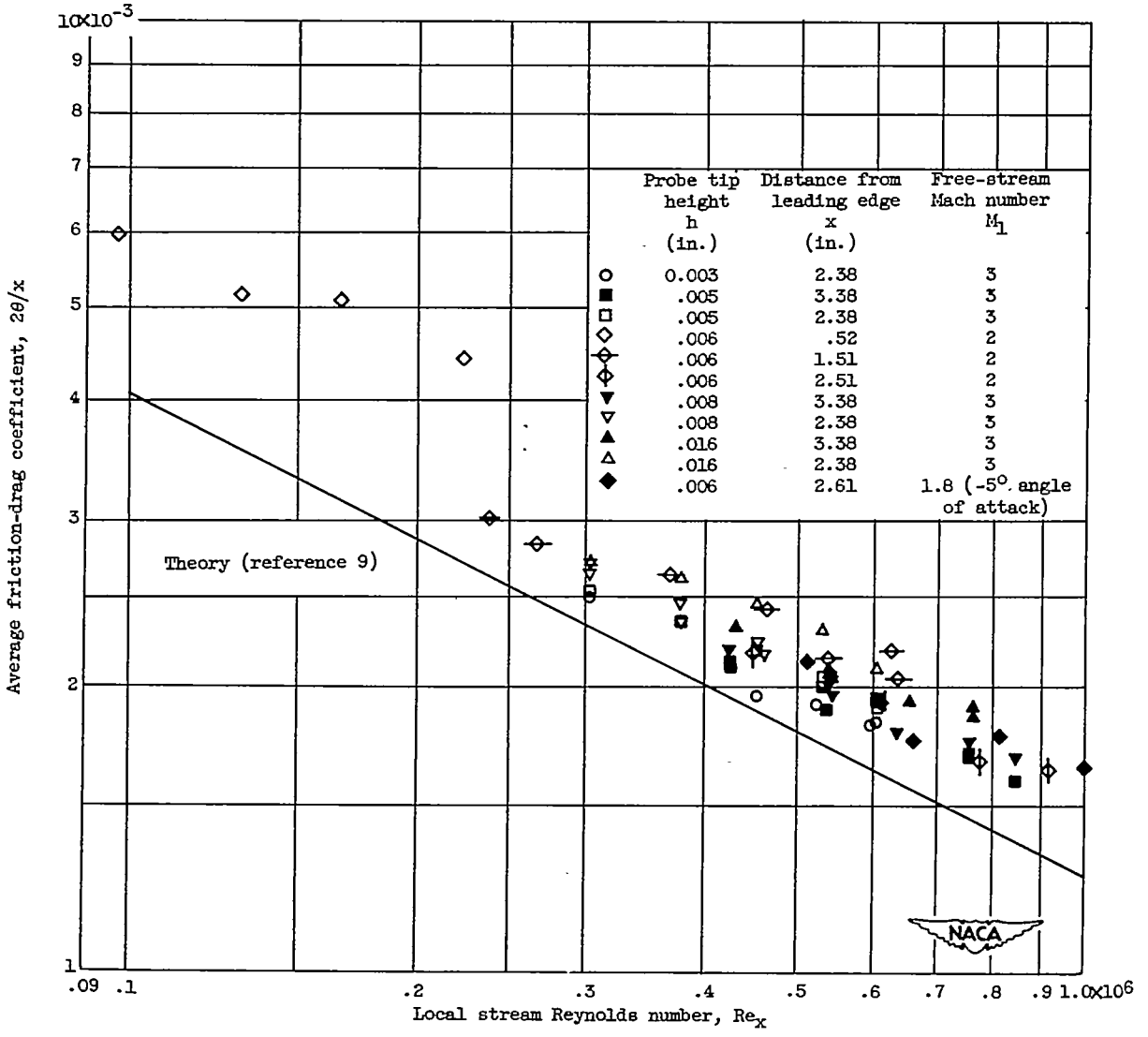

Figure 12. - Average flat plate friction-drag coefficient as function of local stream Reynolds number.

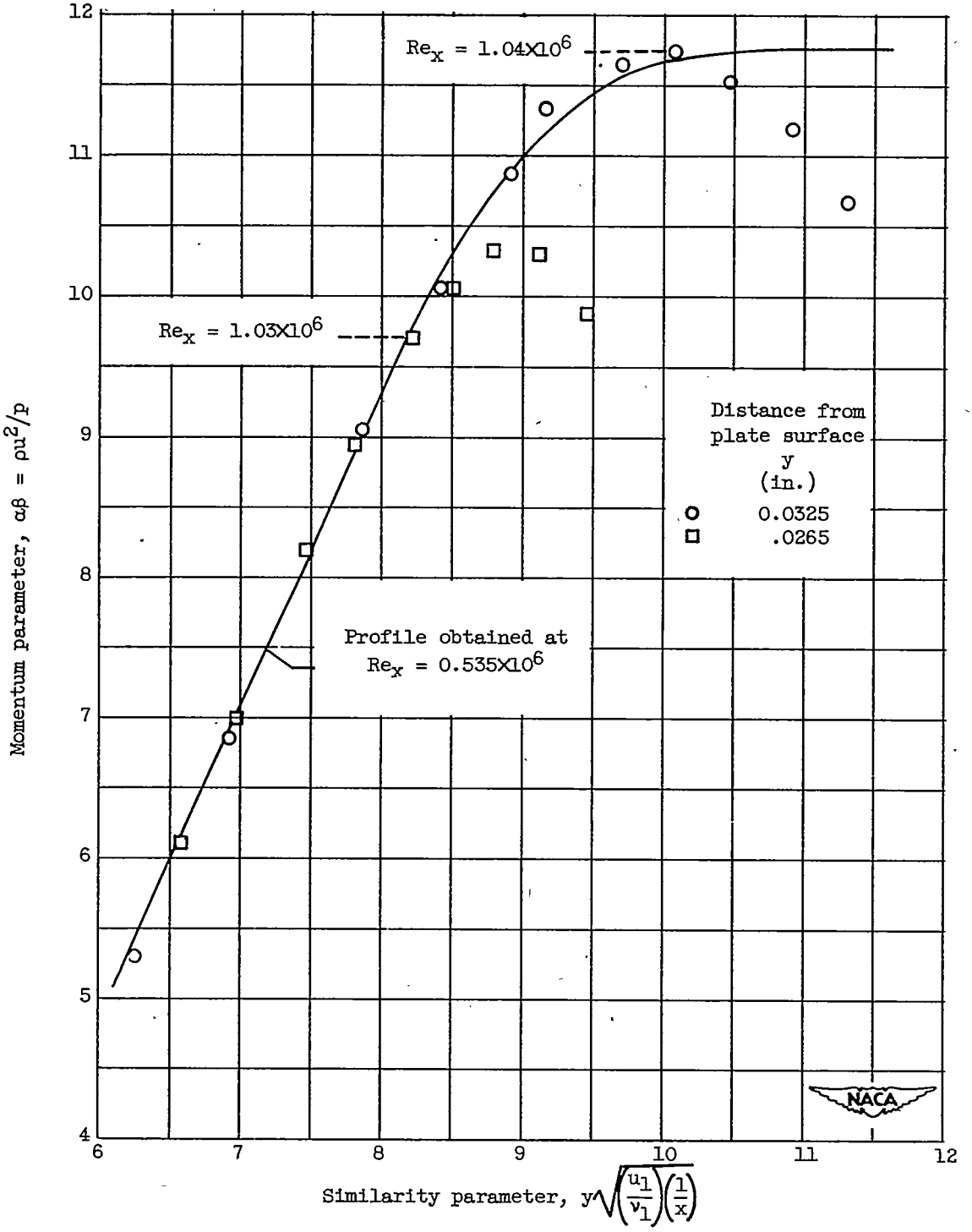

Figure 13. - Curves indicating transition obtained by varying u_1/ν_1 at constant distance from leading edge and from plate surface. Distance from leading edge, 3.38 inches; probe tip height, 0.005 inch; free-stream Mach number, 3.

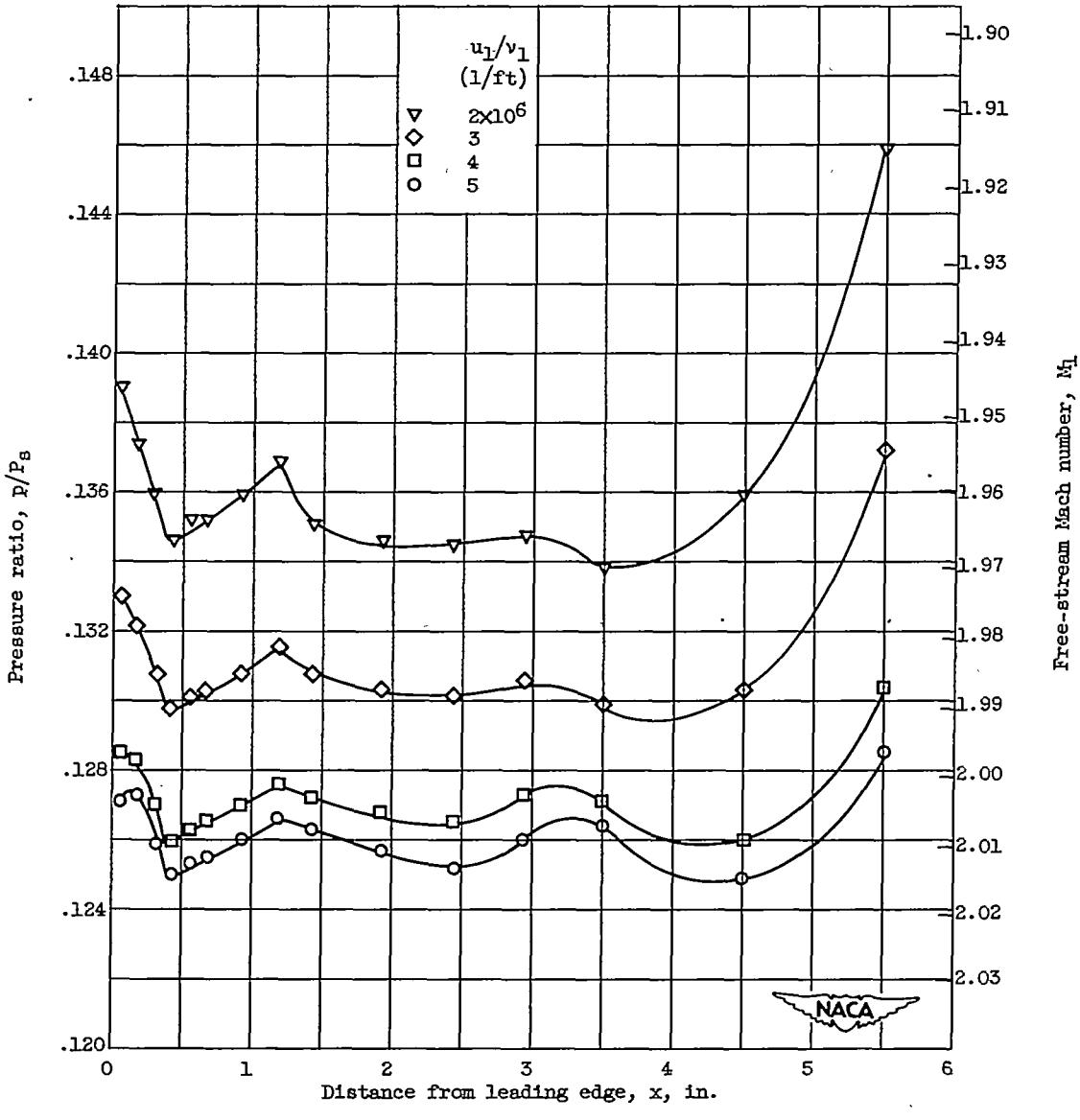

Figure 14. - Pressure distribution on plate in tunnel 1.

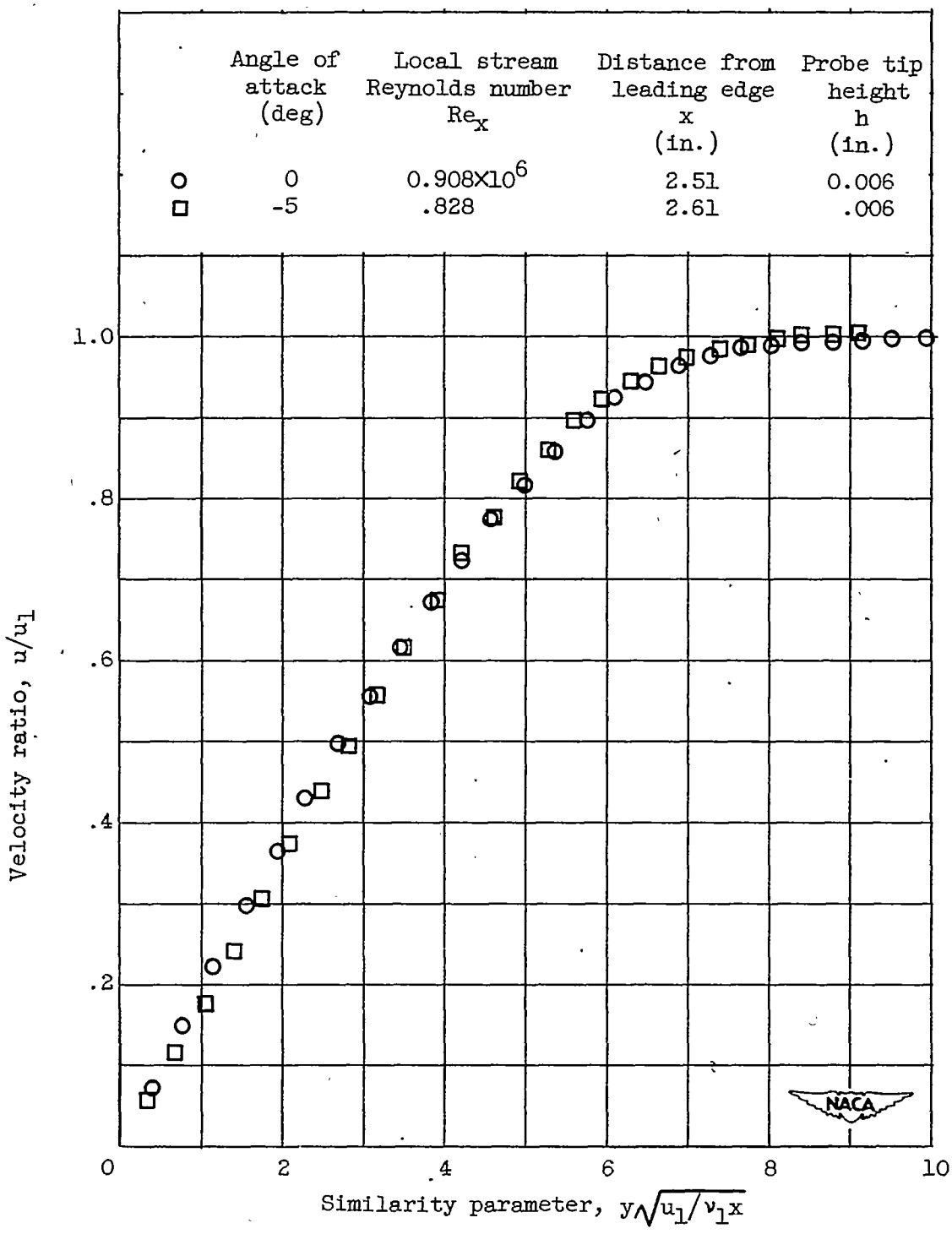

Figure 15. - Typical velocity profiles obtained in tunnel 1 at 0° and -5° angle of attack. Free-stream Mach number, 2.

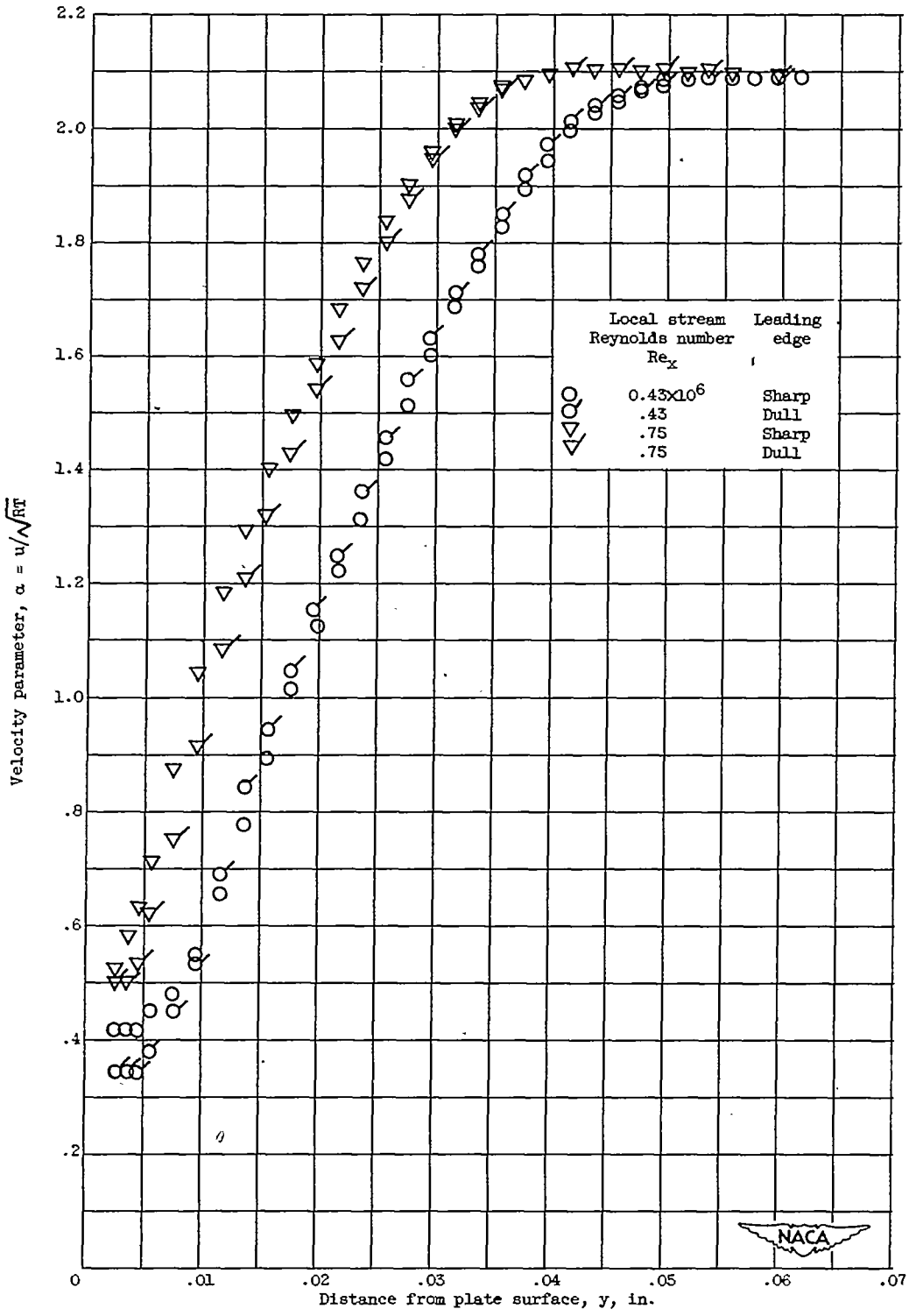

Figure 16. - Velocity parameter profiles with sharp and dull leading edges. Distance from leading edge, 3.38 inches; free-stream Mach number, 3.

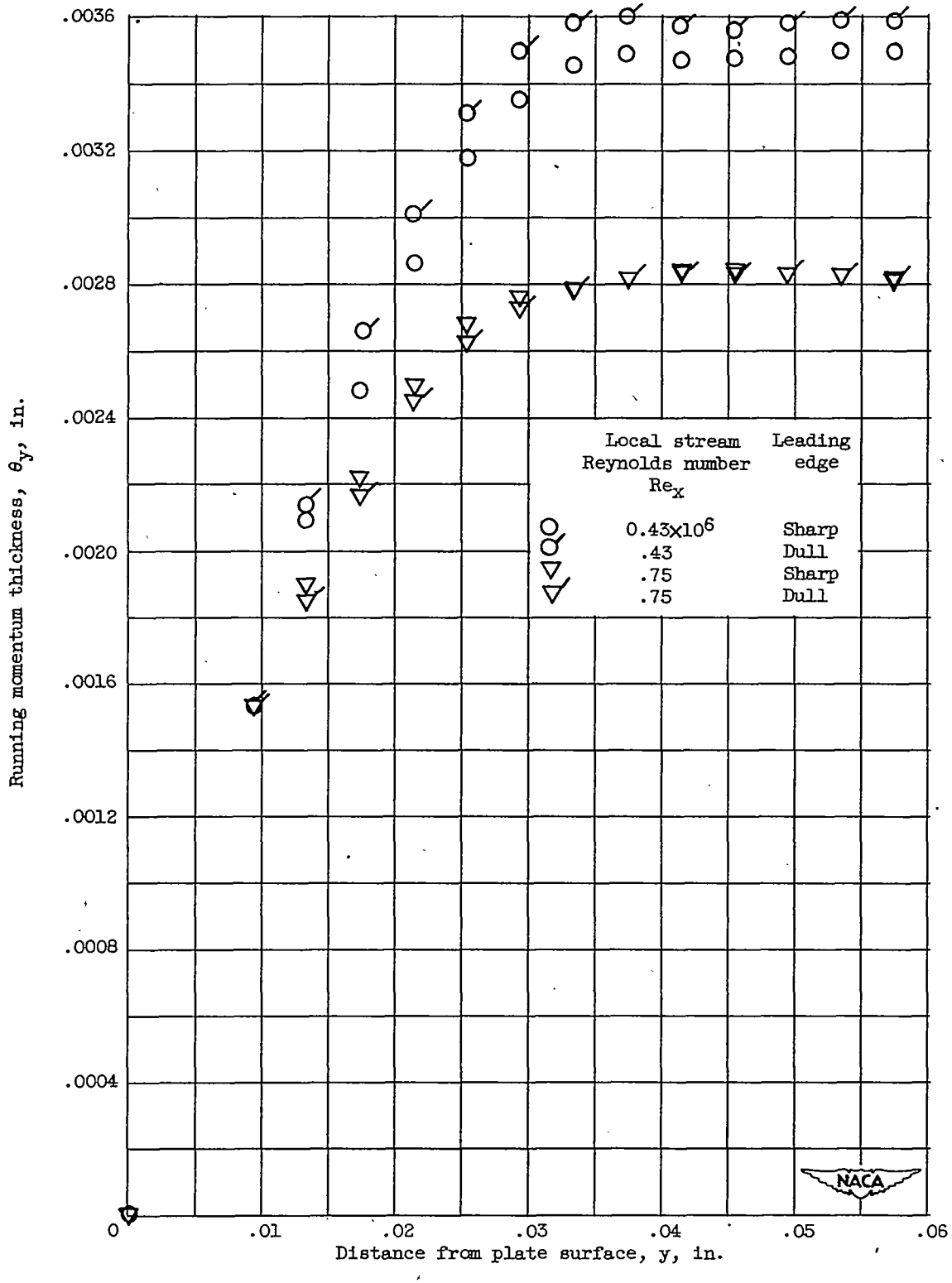

Figure 17. - Momentum thickness profiles with sharp and dull leading edges. Distance from leading edge, 3.38 inches; free-stream Mach number, 3.

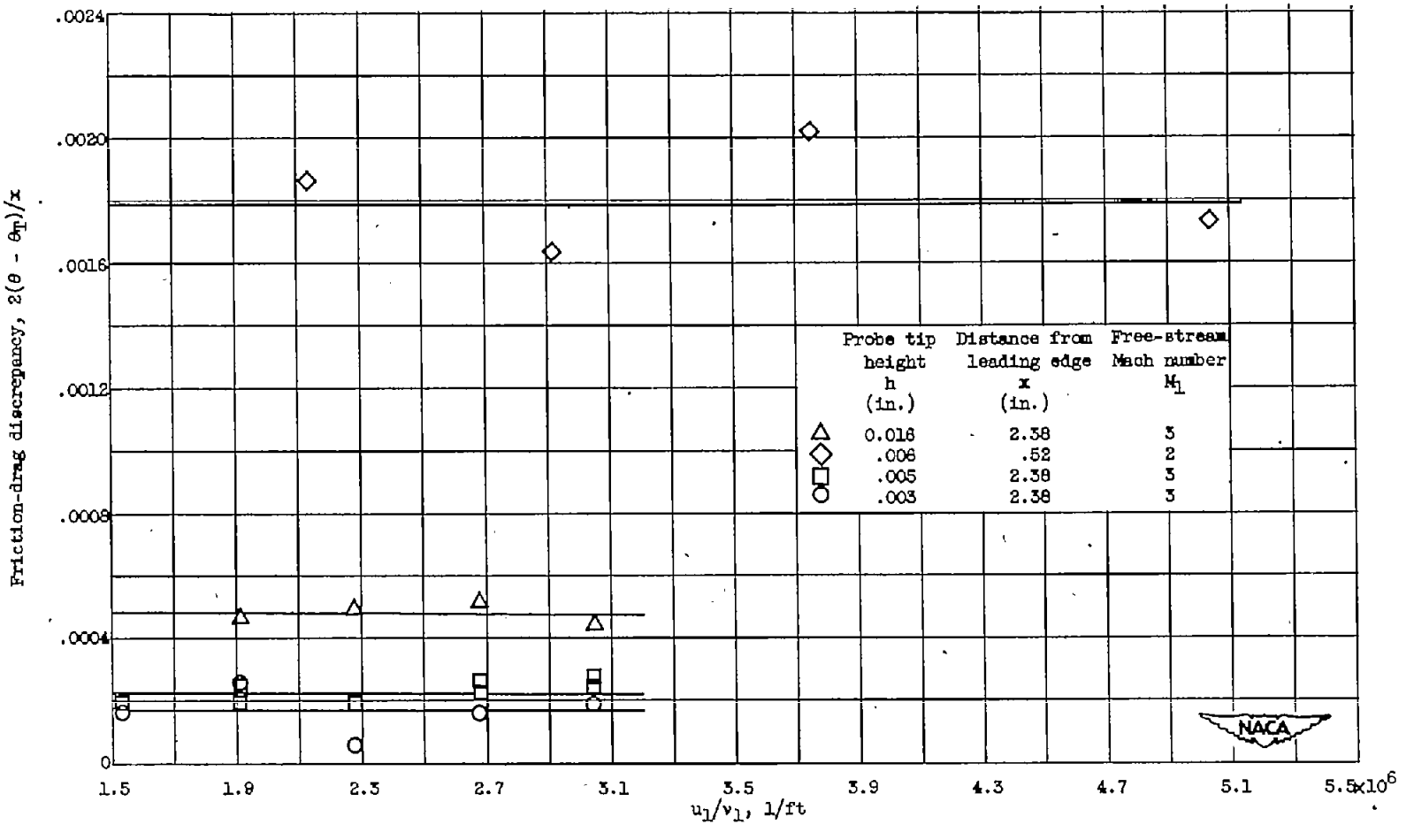

Figure 18. - Friction-drag discrepancy $2(\theta - \theta_T)/x$ as function of u_1/ν_1.

2756

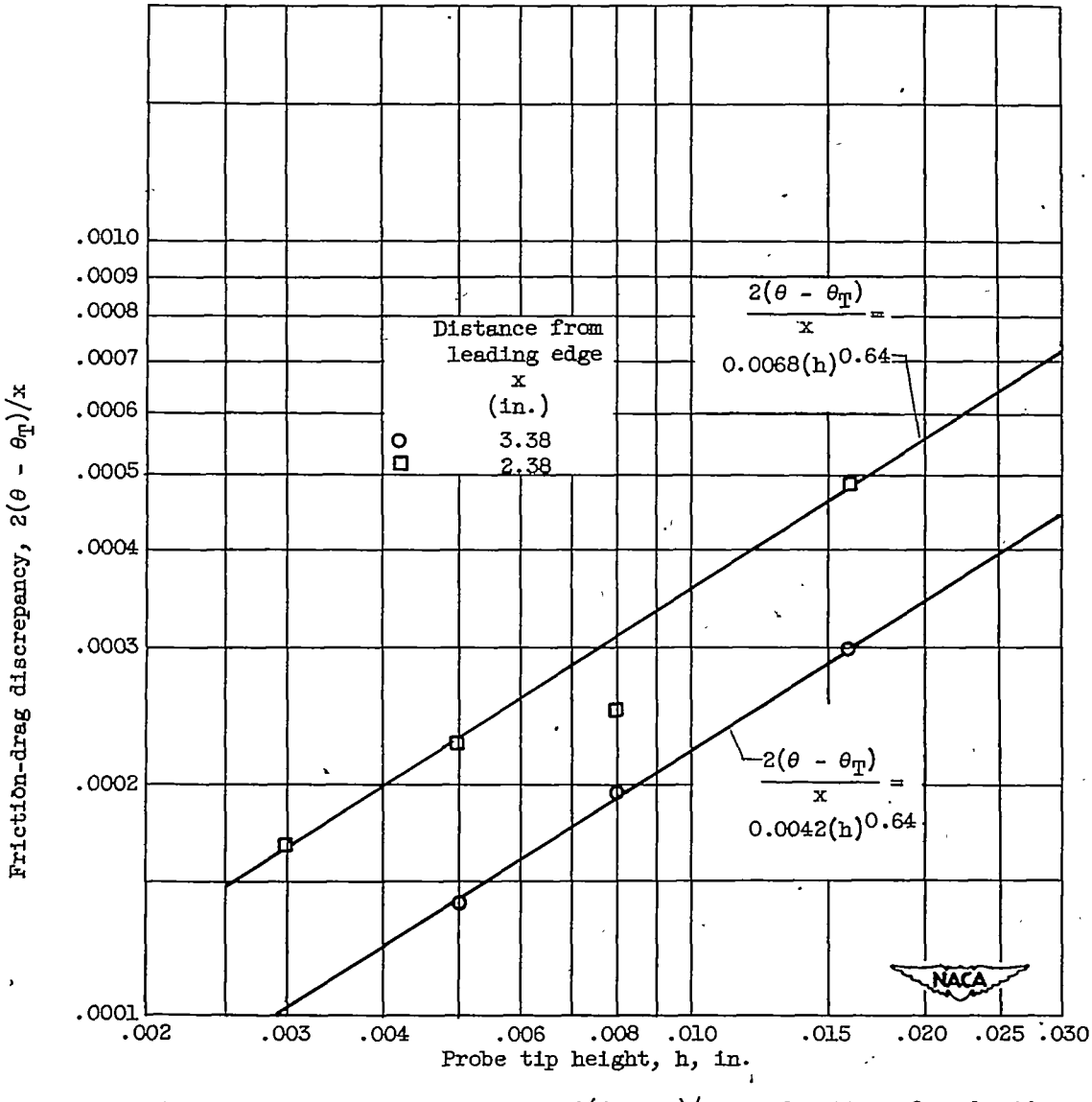

Figure 19. - Friction-drag discrepancy $2(\theta - \theta_T)/x$ as function of probe tip height. Free-stream Mach number, 3.

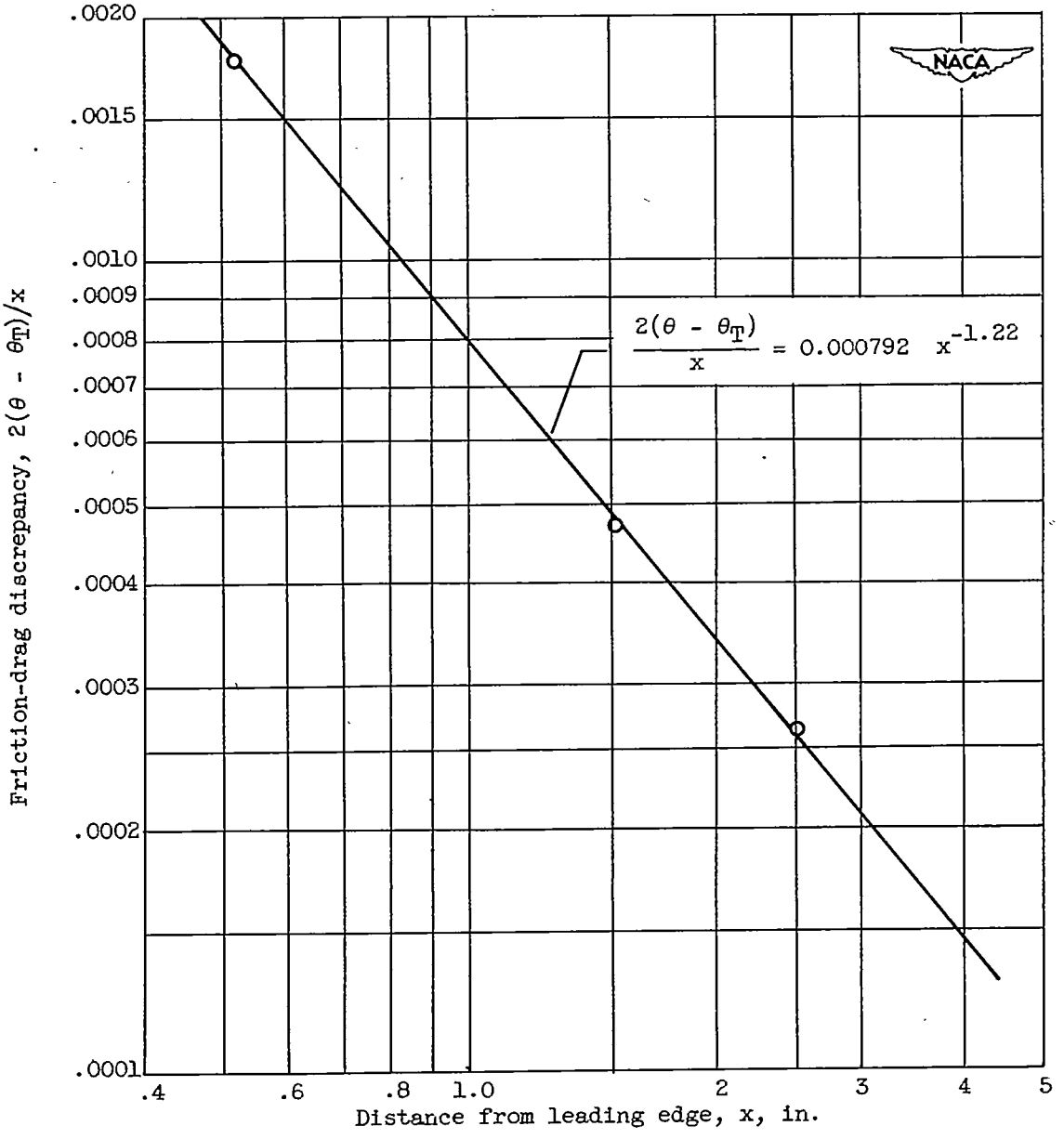

Figure 20. - Friction-drag discrepancy $2(\theta - \theta_T)/x$ as function of distance from leading edge. Probe tip height, 0.006 inch; free-stream Mach number, 2.

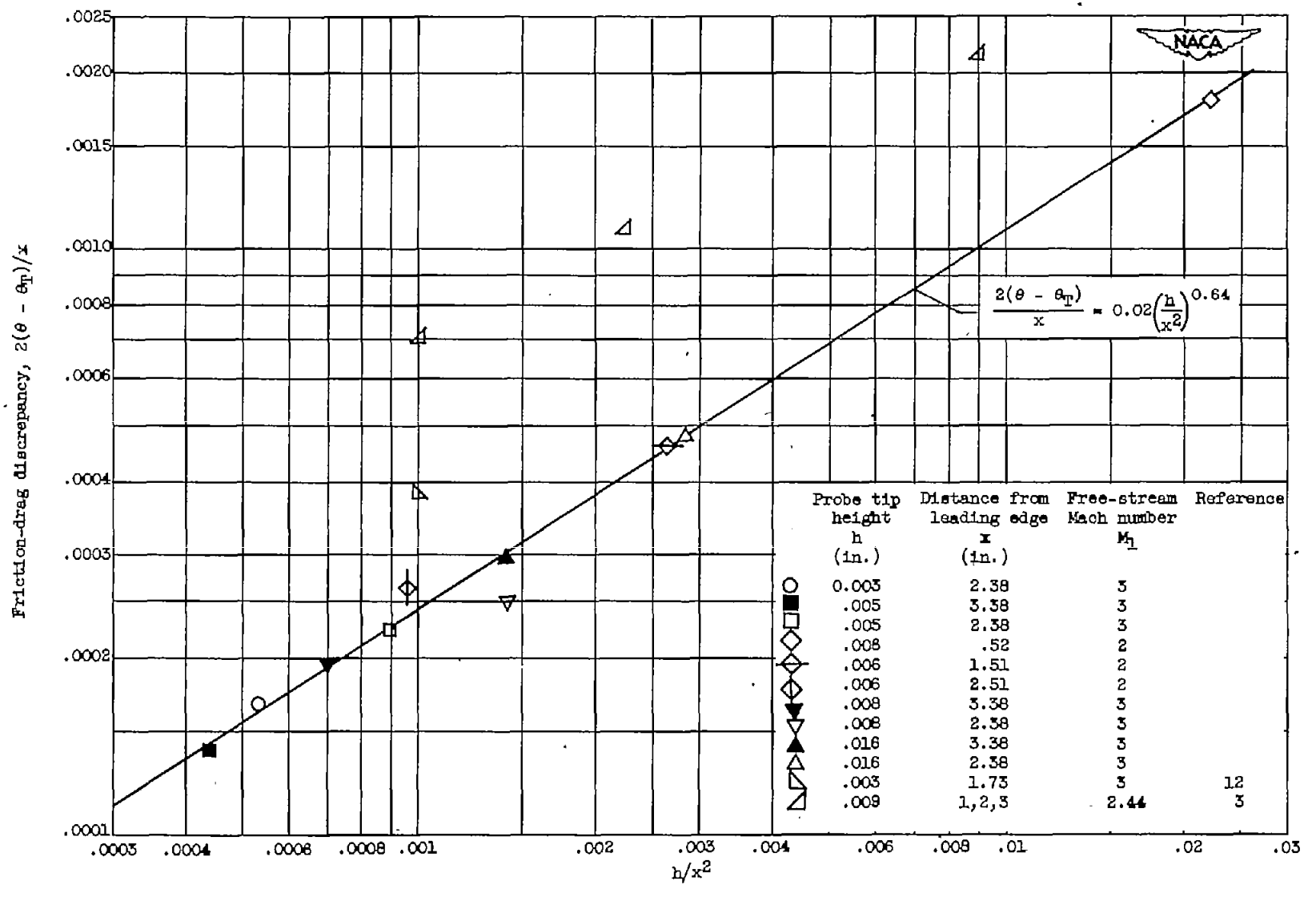

Figure 21. - Friction-drag discrepancy $2(\theta - \theta_T)/x$ as function of h/x^2.

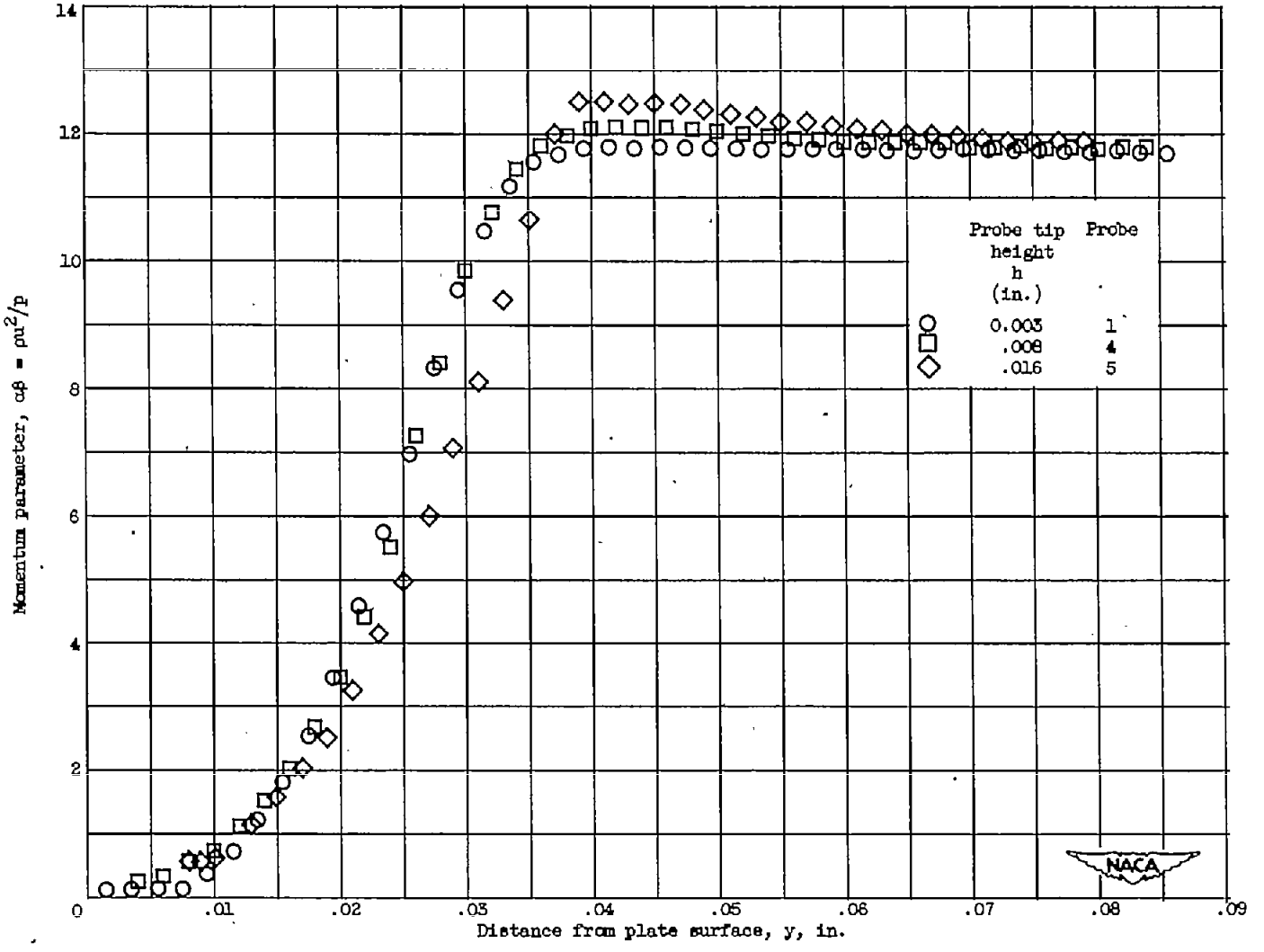

Figure 22. - Momentum parameter profiles for three different probes. Distance from leading edge, 2.38 inches; local stream Reynolds number, 0.45×10^6; free-stream Mach number, 3.

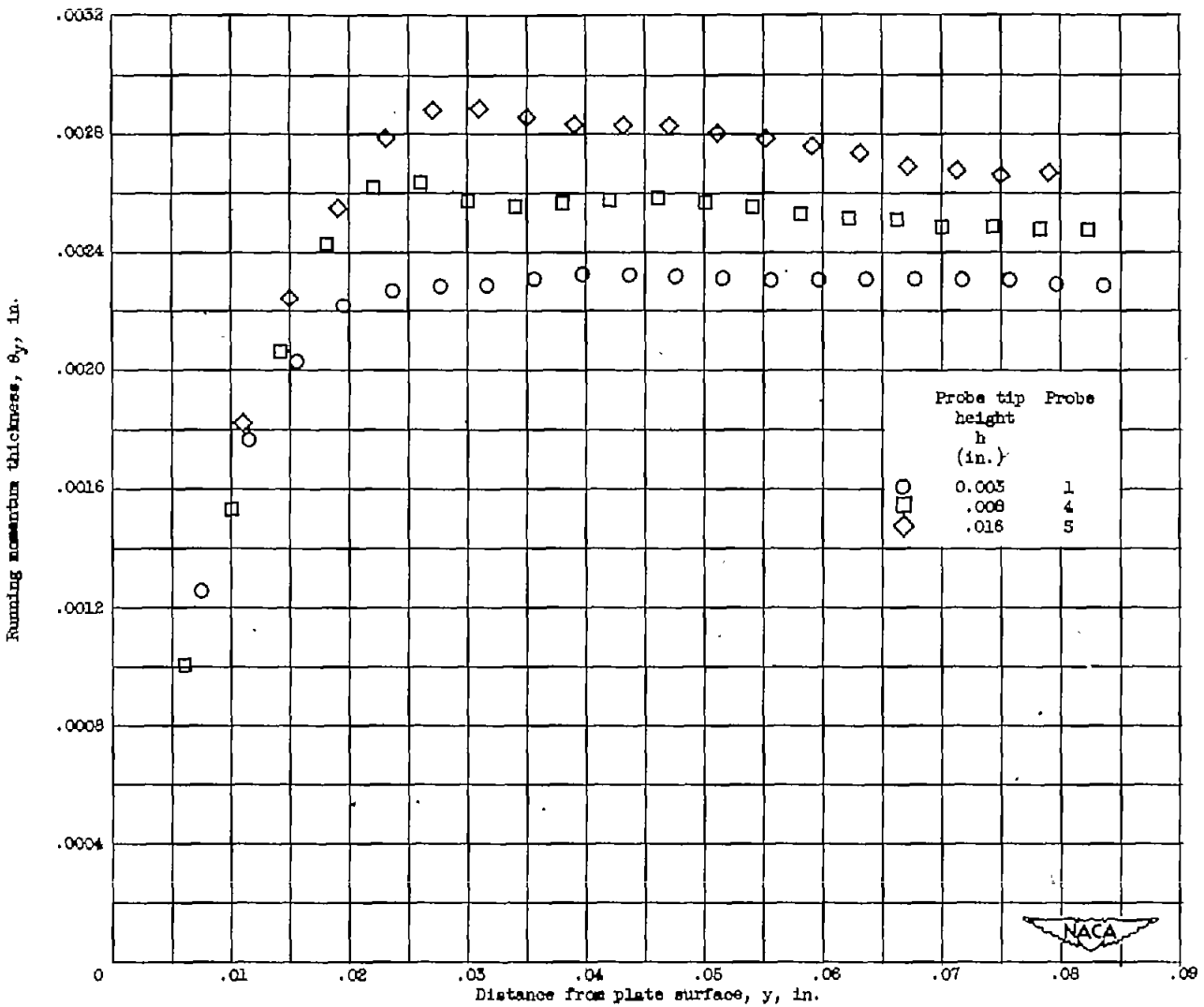

Figure 23. - Momentum thickness profiles for three different probes. Distance from leading edge, 2.38 inches; local stream Reynolds number, 0.45×10^6; free-stream Mach number, 3.

NACA-Langley - 2-16-53 - 1000